Aging alters the mediating effect of endogenous GABA on the interaction between functional connectivity and motor-state transitions.

Kirstin-Friederike Heise[1,2*], Laura Rueda-Delgado[1,3], Sima Chalavi[1,2], Bradley R. King[1,2], Thiago Santos Monteiro[1,2], Richard A. E. Edden[4,5], Dante Mantini[1,6], Stephan P. Swinnen[1,2]

[1] Department of Movement Sciences, Movement Control and Neuroplasticity Research Group, KU Leuven

[2] KU Leuven Brain Institute, Leuven, Belgium

[3] School of Psychology, Trinity College Dublin, Dublin 2, Ireland

[4] The Russell H. Morgan Department of Radiology and Radiological Science, The Johns Hopkins University School of Medicine, Baltimore, MD, USA

[5] F. M. Kirby Research Center for Functional Brain Imaging, Kennedy Krieger Institute, Baltimore, MD, USA

[6] Brain Imaging and Neural Dynamics Research Group, IRCCS San Camillo Hospital, Venice, Italy

*Correspondence to kirstin.heise@kuleuven.be

Abstract

Previous links endogenous gamma-aminobutyric acid (GABA) with behavioral efficiency across perceptual and cognitive domains but with potentially strongest impact on those types of behavior that require a high level of dynamic control. Using a Bayesian moderated mediation analysis, we modeled the age-associated interactions between electroencephalography- and electromyography-derived connectivity metrics and behavior and investigated the specificity of the indirect effect of GABA concentration as measured with magnetic resonance spectroscopy. Only the integrated analysis of all three modalities revealed marked differences between the two age groups. Specifically, relatively lower GABA was more beneficial for the connectivity-behavior association in the young, whereas the older showed a beneficial behavioral effect in the presence of higher GABA given their generally elevated task-related connectivity. Age-related alteration of the preferred state of endogenous GABA concentration may reflect a generic compensatory mechanism allowing for higher temporal precision in neural tuning and maintaining a higher behavioral functioning level.

Introduction

Functional deficits in endogenous γ-aminobutyric acid (GABA)-mediated neural signaling represent one suspect mechanism among the many potential causes of age-related behavioral decline [1]. GABAergic interneurons are suggested to carry a major role in scaling and fine-tuning neural oscillations [reviewed in [2, 3]]. More specifically, GABAergic neurotransmission is believed to be an essential regulator of phase synchronization of neural oscillations [reviewed in [4]], which has been proposed to constitute one of the brain's main modes of communication [5, 6]. Thus, phase-based connectivity indicates the time-sensitive modulation of inter-site neural communication and therefore serves as a proxy for the responsiveness of the neural system.

Previous work indicates that GABA-mediated synaptic mechanisms on cortical level, evaluated at resting-state, predict the system's capacity for dynamic event-related modulation of cortical inhibition, and that this is linked to efficient motor control [7]. This work has led to the hypothesis that, once baseline GABAergic neurotransmission is imbalanced, the system's responsiveness is impaired and this may have detrimental behavioral consequences. Such imbalance may occur at older age when disinhibition becomes more prominent. Experimental evidence for this association between age-related GABAergic dysfunction and declining behavior across perceptual and cognitive domains points towards stronger impact on those types of behavior that require a high level of dynamic control [e.g. [8–10]]. Lowered motor cortical GABA levels, on the other hand, are found to correlate with age-related changes in sensorimotor connectivity and diminished motor control [11]. These recent findings suggest a broader link between GABA availability and connectivity as a read-out for neural communication with implications for behavioral efficiency. However, whether these phenomena are simply co-occurring or whether they can be attributed to underlying causal mechanisms remains an open question.

To test this neurochemical - neural communication - behavioral framework in the light of healthy ageing, we employed a multimodal approach to fuse baseline GABA levels with the dynamic modulation of cortico-cortical and cortico-spinal phase synchronization in the context of motor-state transitions in neurotypical young and older volunteers. The control of transitions between dynamical

motor states of varying complexity has shown to engage widespread, and in particular interhemispheric, neural communication within the sensorimotor system [e.g. [12, 13]] and was therefore selected as task paradigm to address this question.

We hypothesized age-associated lower endogenous GABA levels to impact cortico-cortical communication specifically, and therefore probed it against cortico-spinal connectivity. Since the cortico-spinal connectivity underlies other modulating influences (e.g. Renshaw cells on spinal level) downstream [e.g. [14, 15]], we expected it to show less sensitivity to individual variations in baseline cortical GABAergic mechanisms than cortico-cortical connectivity. In line with the framework introduced above, we assumed that age-related alterations of neural communication would consequently manifest in distinct behavioral declines.

Results

To investigate the impact of individual variations in baseline GABA levels for the association between functional cortex-cortex and cortex-muscle coupling and complex bimanual behavior we used a cross-sectional multimodal approach. The participants underwent three sessions involving magnetic resonance spectroscopy (MRS) to extract endogenous GABA levels, electroencephalography (EEG) and electromyography (EMG) during motor state transitions to compute functional cortex-cortex and cortex-muscle coupling and behavioral parameters (Figure 1, see Materials and Methods section for details). Each of these modalities were (neurochemical, neural, behavioral) were first analyzed unimodally and then integrated with a Bayesian moderated mediation analysis to investigate the interaction among the modalities.

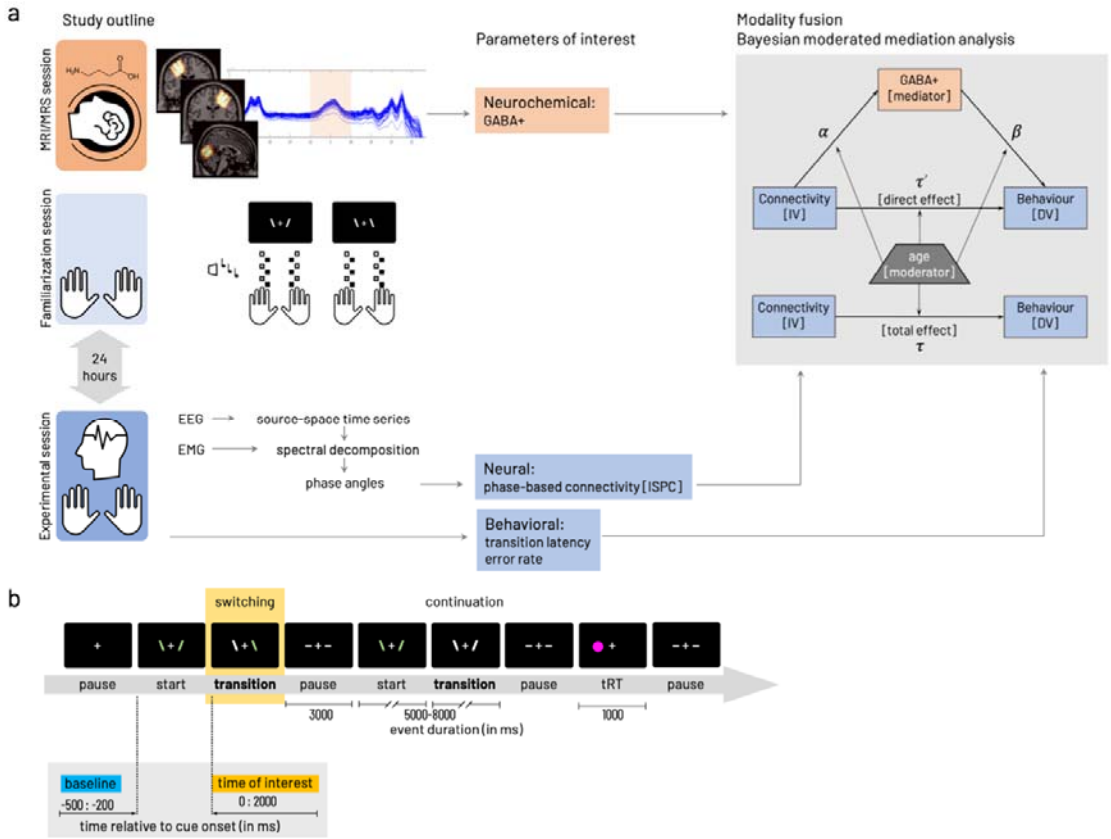

Figure 1: Experimental procedures and parameters of interest. a) Study outline *with MRI/MRS session, task familiarization preceding the experimental session including EEG during task performance. Edited MRS and T1-weighted images were used to extract tissue-corrected GABA levels and additional macromolecules (GABA+) from left and right primary motor and occipital voxels. The behavioral paradigm involved transitions between a stable (mirror-symmetric in-phase tapping, left) and a less stable (anti-phase tapping, right) motor state. Task familiarization included stimulus-response mapping and individual performance frequency adjustment. Performance in motor state transitions was described with transition latency and error rate. EEG/EMG was recorded during the main experiment and used to compute connectivity (inter-site phase clustering, ISPC) between left and right primary motor sources and between cortical sources and intrinsic hand muscle activity. The parameters of interest from the individual modalities were integrated with a Bayesian moderated mediation analysis estimated for cortico-cortical connectivity and for cortico-spinal connectivity as independent variable [IV]. In both cases, dependent variable [DV] behavior was either median transition latency or cumulative error rate. Details on formalization of model paths* $\alpha, \beta, \tau', \tau$ *given in Methods.* ***b) Flow of events within the main experiment.*** *Phases of finger movement ('start', 'continuation', 'switching') were interleaved with rest phases ('pause'). A randomly occurring reaction time task ('tRT'), a fast key press with either left or right thumb in response to appearance of a circle on the side of the required response was interspersed with the other events with a 5% probability of occurrence. Inlay highlights the time zones relevant for the EEG/EMG data analysis. Data collected in the within-trial pause (demarked in blue) was used as baseline for the EEG/EMG analysis of the data from the time of interest (yellow).*

GABA-MRS

MRS data from left, right M1 and occipital voxels were acquired in 22 older and 22 young participants. In two cases (one older, one young), the data of the right M1 were excluded from further analysis due to motion artifacts and insufficient model fit.

A gamma GLMM (identity link) was fitted to predict GABA+ with group (young, older), voxel (left M1, right M1, OCC), and to identify the influence of the quality metrics (GABA SNR, GABA Fit Error, NAA SNR, Drift, Frequency Offset (mean-centered) and NAA FWHM) and their potential interaction with voxel or group (Figure 2a). Quantitative quality metrics (for descriptive statistics see S1 Table) are comparable to those published in recent studies from our and other groups [16–18]. Consistency of the voxel placement across participants and individual traces of edited spectra for each voxel were visually inspected (Figure S1).

Stepwise backward selection revealed that none of the quality metrics was influenced by the main variables of interest being group or voxel, and revealed that only Frequency Offset and GABA SNR significantly explained overall variance in the data (Table S2) and were therefore included in the final model (Figure S3). We found an overall average GABA+ level at 2.39 i.u. as indicated by the final model's intercept (SE = 0.292, 95% CI [1.81, 2.96], $p < .0001$). GABA+ was found to be significantly different across voxels and this effect was significantly modified by factor group (overview of effects given in Figure 2b, parameter estimates and Wald statistics for GLMM predicting GABA+ given in Table S3 together with summary of marginal means contrasts). This group × voxel interaction was mainly explained by within-group differences between lower GABA+ levels in sensorimotor voxels as compared to the occipital voxel in young adults. Although the older tended to have larger differences between GABA+ levels in the sensorimotor and occipital voxels, there were no group differences for the individual voxels (all $p > .1$). Moreover, there were no within-group hemispheric differences for sensorimotor voxels (all $p > .1$).

In short, the main finding of the analysis of the tissue-corrected GABA+ levels showed reduced GABA+ levels in the sensorimotor voxels compared to the occipital voxel, which was visible in both age groups.

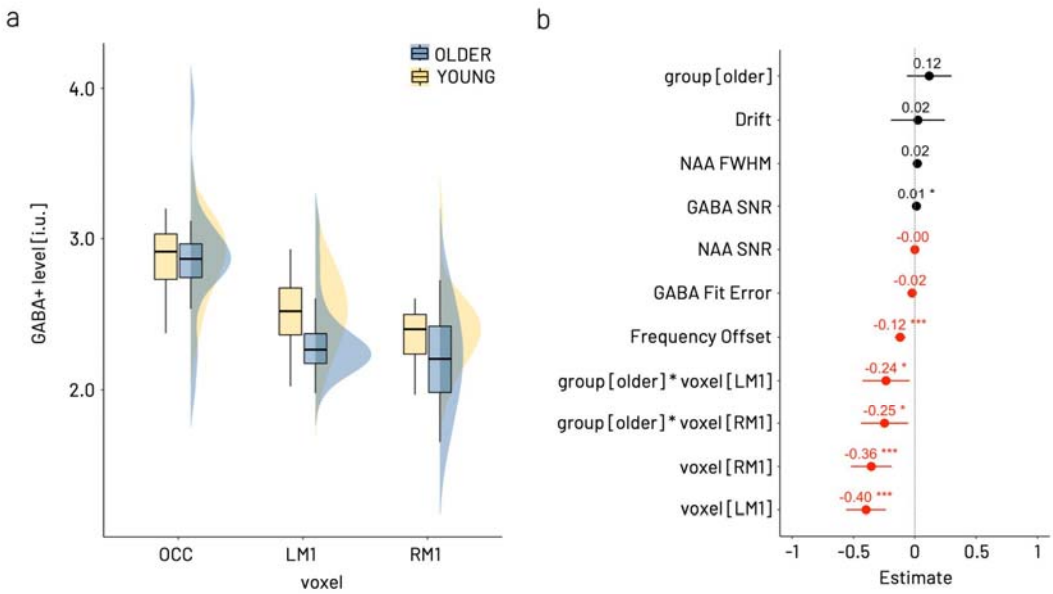

***Figure 2 GABA MRS results**. **a)** Boxplots (see Material and Methods for represented group statistics) and distributions shown for the interaction effect of group and voxel is driven by the within group differences between sensorimotor voxels compared to the occipital voxel. **b)** Forest plot of parameter estimates for the statistical model fitted to predict GABA+. Depicted estimates for parameters are shown in relation to reference categories (group[young], voxel[occipital]). Red color codes negative and black codes positive effects on odds ratio. Asterisks indicate significant effects at *p<.05, ** p<.001, ***p<.0001.*

Behavior

The control of transitions between motor-states was tested with a variation of an established paradigm [19–22], in which the participants had to rhythmically tap with the index and middle fingers of both hands and to control transitions between two coordinative patterns of different complexity (Figure 1a, see Methods for details of the behavioral paradigm). The behavioral data collected during the performance of the behavioral paradigm was analyzed in a time window of 2000ms following the 'continuation' or 'switching' cue with two main aims: (1) to quantify the precision of performance (error rate) and (2) to quantify the speed of performance (transition latency). The time window of interest for these parameters was based on previous work [22] and pilot testing in older participants with the same task. Together these data revealed that change in coordination mode is realized over an extended period and not a discrete event in time. Furthermore, a simple binarization of the precision (correct – wrong) does not reflect the ongoing adjustments made until the new coordination mode is

mastered. On average, 144 trials per participant were subjected to the analysis. Summary statistics of the behavioral outcome parameters of the bimanual transition task are given in Table 1.

Table 1 Summary statistics of outcome parameters of the bimanual transition task

	Total Trials	*Failed Transitions*	*Fully correct transitions*	*Cumulative error rate [in %]*				*Transition Latency [in ms]*			
GROUP	*N*	*N*	*N*	*mean*	*Sd*	*median*	*ci*	*mean*	*sd*	*median*	*ci*
young	3023	93	389	16.44	14.60	13.33	0.57	553.83	284.56	580	10.34
older	3168	235	568	18.73	17.96	14.09	0.76	759.76	414.9	758	15.62

Error rate

An overview of the distribution of error rate across age groups, transition conditions, and coordination patterns is depicted in Figure 3a. To capture a comprehensive picture of performance during the transition phase, we chose to split the precision measure into three distinct levels, namely, *fully correct transitions* representing trials showing 100% correct tapping, *failed transitions* reflecting trials with 100% of erroneous tapping, and *cumulative error rate* consisting of all remaining trials not considered fully correct or failed.

Failed transitions [trials with 100% error rate]. A logistic GLMM was used to predict failed transitions using group [OLDER, YOUNG], transition condition [continuation, switching], coordination pattern [IP, AP], and number of trials as independent variables (overview of effects given in Figure 3b, results summarized in Table S4, conditional R2 = 0.61, marginal R2= 0.08). The overall odds of completely failing a transition were very low with 0.002 (intercept: beta = -6.17, SE = 0.75, 95% CI [-7.64, -4.69], $p < .001$). Trial number turned out to be the only significant effect showing that with each additional trial, the odds of completely failing the transition were reduced by 0.82 (beta = -0.20±0.07, 95% CI [-0.34, -0.06], $p = 0.005$). Most importantly, these results show that there was no difference in failed transitions between older and young.

Fully correct transitions [trials with 0% error]. In analogy to *failed transitions*, a logistic GLMM was fitted to predict fully correct transitions (Figure 3c, summary of results in Table S5, conditional $R^2 = 0.41$, marginal $R^2 = 0.35$). After removing failed transitions from the data, the overall odds for trials to be fully correct were 2.733 (intercept: beta = 1.01, SE = 0.20, 95% CI [0.62, 1.39], $p < .0001$). Compared to continuation transitions, switching transitions were less likely to be fully correct (transition condition [switching]: odds ratio = 0.02, beta = -3.93±0.19, 95% CI [-4.31, -3.56], $p < .001$). The AP coordination pattern was less likely to result in fully correct transitions (coordination pattern [AP]: odds ratio = 0.33, beta = -1.09±0.22, 95% CI [-1.52, -0.67], $p < .001$). Age group was a significant effect modulator, i.e. switching transitions were more likely to be fully correct in the older (group [OLDER] * transition condition [switching]: odds ratio = 2.33, beta = 0.85±0.25, 95% CI [0.35, 1.35], $p < .001$). Likewise, age group modulated the interaction effect of coordination pattern and transition condition (beta = 0.84±0.40, 95% CI [0.05, 1.63], $p = 0.037$). This triple-interaction effect was mainly driven by the higher likelihood of older participants to produce fully correct switching transitions and the IP coordination pattern being more likely to be fully correct in both groups and transition conditions (see marginal means contrasts below Table S5).

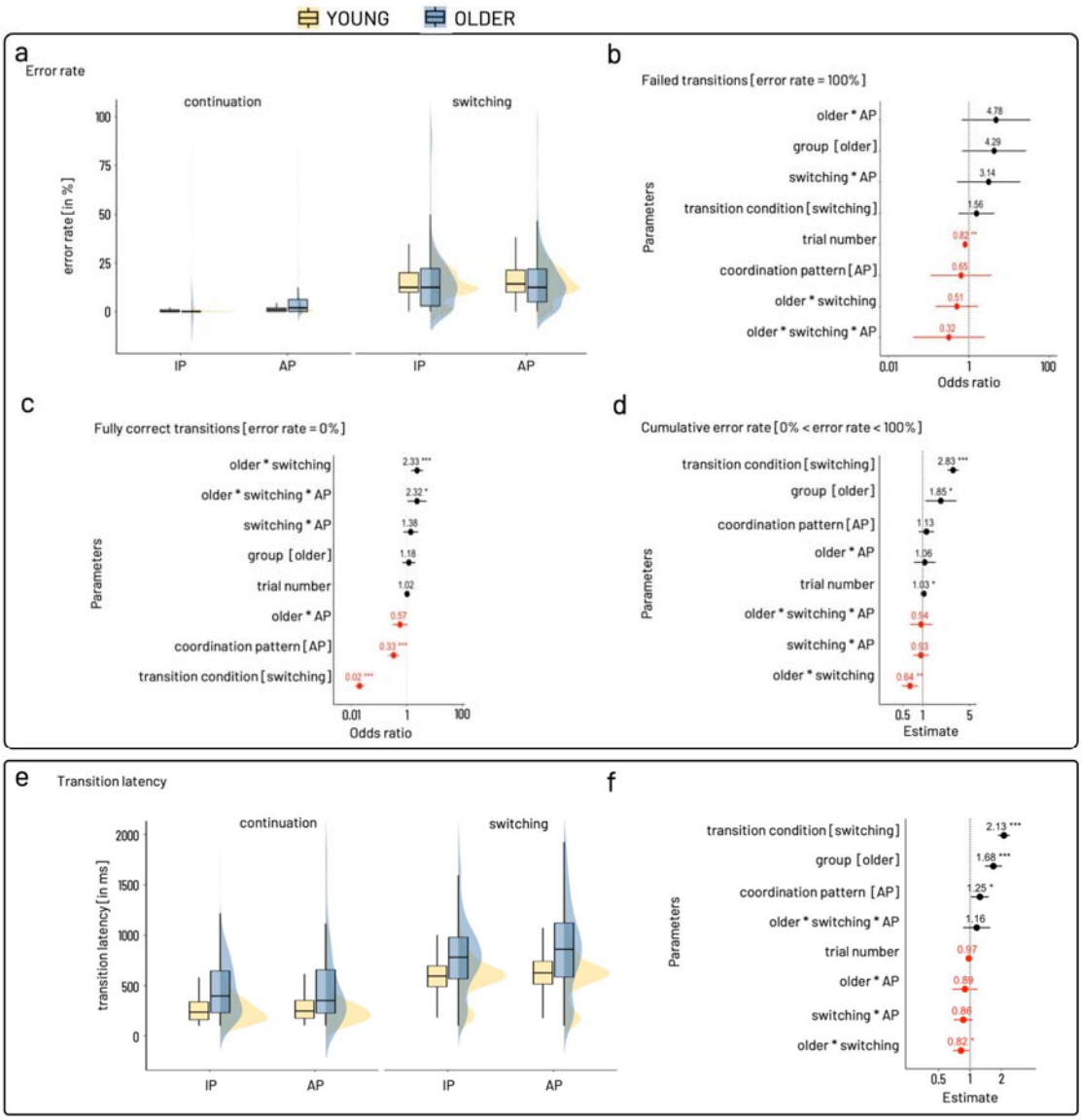

Figure 3 Predictors for behavioral outcome. a-d) Error rate. a) *Boxplots and distributions for error rate given for separate transition conditions (continuation vs. switching) and coordination patterns (IP: in-phase, AP: anti-phase) within age groups (blue: older, yellow: young).* ***b)*** *Forest plot of parameter estimates for the statistical model fitted to predict failed transitions, i.e. error rate = 100%. Depicted odds ratio for parameters are shown in relation to reference categories (group[young], transition condition [continuation], coordination pattern [IP]). Red color codes negative and black codes positive effects on odds ratio. Numbers indicate effect sizes and asterisks indicate significant contrasts based on marginal means.* ***c)*** *Forest plot of parameter estimates for the statistical model fitted to predict fully correct transitions. Depicted parameter levels are shown in relation to reference categories, notation, and color coding as in b.* ***d)*** *Forest plot of parameter estimates for the statistical model fitted to predict cumulative error rate. Notation, and color coding as in b).* ***e-f) Transition Latency. e)*** *Summary statistics for transition latency. Color coding as in a).* ***f)*** *Forest plot of parameter estimates for the statistical model fitted to predict transition latency. Depicted parameter levels are shown in relation to reference categories, notation, and color coding as in b. Asterisks indicate significant effects at *p<.05, ** p<.001, ***p<.0001.*

Cumulative error rate [0<error rate/100 <1]. A beta GLMM (logit link) was fitted to predict cumulative error rate including the same parameters as described before (overview given in Figure 3d, summary of results in Table S6, conditional R^2 = 0.68, marginal R^2 = 0.056). After excluding fully correct and fully erroneous transitions [0<error rate/100 <1], an overall proportion of 7.5% of cumulative error rate was found (intercept: beta = -2.59, SE = 0.195, 95% CI [-2.97, -2.21], p < .0001). Overall, the older produced a 1.85 times higher cumulative error rate (beta = 0.617±0.274, 95% CI [0.08 1.15], p = 0.024). Compared to continuation, switching transitions increased the proportion of cumulative error rate by 2.834 times (beta = 1.04±0.0975, 95%CI [0.851 1.23], p <.0001). The interaction effect of age group and transition condition showed a 0.64 times proportional reduction in cumulative error rate during switching transitions in the older (beta = -0.453±0.144, 95%CI [-0.734 -0.171], p<.01). This effect was primarily explained by significantly lower cumulative error rate in continuation transitions in both groups while the young showed significantly lower errors in continuation but not switching transitions (see below Table S6 for summary of marginal means contrasts). With each additional trial (nTRIALc), cumulative error rate significantly increased by 1.27 times (beta = 0.0262±0.0115, 95%CI [0.00358 0.0488], p < .05).

Transition Latency

The transition latency was defined as the time delay between cue onset and valid response, i.e. the first occurrence of the correct coordination pattern indicated by the cue. Importantly, *failed transitions* were excluded from the trials for the calculation of the transition latency. To be valid, correct responses to visual cues had to have a latency ≥100ms and <2000ms, in order to allow for visual processing of the cue and visuomotor integration for the correct response [23–25]. An overview of the distribution of transition latency across age groups, transition conditions, and coordination patterns is depicted in Figure 3e. A GLMM (Gamma family with a log link) was fitted to predict transition latency with the same independent variables described for error rate (model effects overview depicted in Figure 3f, summary of results in Table S7, conditional R^2 = 1.00, marginal R^2 = 0.94). The model's intercept at 5.59 on the log scale corresponds to 267.56ms of overall transition latency (SE = 0.07, 95% CI [5.45, 5.72], p < .001). Older performed on average 1.68 times slower (beta = 0.52±0.10, 95%

CI [0.33, 0.71], $p < .0001$). Compared to continuation, switching transitions were 2.13 times slower (beta = 0.75±0.07, 95% CI [0.62, 0.89], $p < .0001$). Overall transitions into the AP pattern were 1.25 times slower than transitions into IP (beta = 0.22±0.10, 95% CI [0.02, 0.42], $p = 0.028$). Transition condition significantly modified the effect of age group (beta = -0.20±0.09, 95% CI [-0.38, -0.02], $p < 0.05$), which meant that continuation transitions were generally faster in both groups and young were faster for both transition conditions. Overall, transitions became faster over time (nTRIALc), though not significantly (beta = -0.03±0.01, 95% CI [-0.05, 0.00], $p = 0.054$).

In summary, the three aspects defining the quality of performance in the complex bimanual paradigm used here (namely failed transitions, fully correct transitions, and cumulative error rate) and the speed of performance (i.e. the transition latency) reflected the age-related performance decline in defined domains only. While the results of increased transition latency confirm an expected slowing in the older group, the results show a comparable level of performance concerning the quality of transition performance in the two age groups, which was the goal of the paradigm adjustment used here.

Overall, continuation transitions were less erroneous and faster than switching transitions, irrespective of coordination pattern and age group reflecting the disadvantage of switching, commonly known as switching costs [26]. However, the older adults showed overall more erroneous performance during continuation trials. This may partly be explained by the lower number of continuation transitions, which may have induced an additional surprise effect hampering the otherwise easier condition of continuing the already performed pattern. Previous work has shown that, even in continuation transitions, the visual cue induces a short interruption of performance [27]. It is possible that this effect was amplified in the older adults due to the general challenge of the switching transition, which may have resulted in a stricter focus on the control of the transition event per se and hence may have additionally increased intentional conflict, i.e. potential interference of the previous switching task-set, in the case of continuation trials [28].

Importantly, the results also support a fairly stable level of performance throughout the length of the experiment in both groups even though the very low likelihood of failed trials decreased even further

over time and a slight increase in cumulative error rate hints at a minimal loss of precision over time. Additional support for stable task performance comes from the results of the thumb reaction task (Table S8), which showed no effect of time across the experiment, suggesting that a comparable level of attention was preserved across the experiment in both age groups. At the same time, the results may indicate an additional small positive training effect with less failed and overall faster transitions, despite the familiarization session prior to the experiment.

For subsequent analysis steps, trials of *fully correct transitions* and *cumulative error rate* were recombined into *error rate*, i.e. *failed transitions* were not considered for further analysis.

Task-related modulation of connectivity (ISPC)

Phase-related connectivity (inter-site phase clustering, ISPC) between motor-cortical source signal and the signal from intrinsic hand muscles was analyzed in N=20 young and N=22 older participants (see Methods for details).

Response-locked analysis of task and group related connectivity (ISPC) modulation.

No significant clusters were found for the interaction of group and task condition. Subsequently, separate contrast analyses were performed to evaluate the effects of age group [YOUNG - OLDER] and task condition [IP – AP].

Group Contrast [YOUNG – OLDER]

Left M1 – right M1

A cluster showing a significant relative decrease of connectivity between the homologue M1 sources was evident for the high alpha to high beta frequency ranges (12-38Hz) starting from -160ms and lasting until 220ms relative to the response (Figure 4, upper panel). This effect was driven by a strong reduction in connectivity in the young while the older showed an increased connectivity overall but also when divided into separate time × frequency sub-clusters, reflecting pre-/post transition time zones and conventional frequency sub-bands. The sub-clusters spanned the ranges pre-transition high beta, peri-transition low beta, and post transition high alpha/mu frequency range (Figure 4, clusters A-C).

Left M1 – right FDI

In the dominant cortico-spinal connection, there were two defined clusters mostly expanding over the pre-transition time window (Figure 4, middle panel). In the pre-transition mu to beta range (14-26Hz, cluster D), a relative decrease in connectivity manifested between -260 to –60ms before the response. While the younger tended to decouple in this frequency range, the older showed increased connectivity. In the theta to alpha range (5-12Hz), a relative increase in connectivity was evident from -260 to 80ms relative to the response (cluster E). This effect was driven by a stronger increase in connectivity strength in the young group.

Right M1 – left FDI

For the non-dominant cortico-spinal connection, an early and a late cluster appeared in the lower frequency range. In the beta frequency range a significant cluster was demarked closely around the response (Figure 4, lower panel). In the theta and alpha frequency range (5-12Hz), a relative connectivity increase expanded from -260 to 50ms relative to the response. This effect was caused by a relatively stronger increase in connectivity in the young (cluster F). The connectivity modulation in the beta range was temporally and frequency-wise selectively defined with an earlier connectivity increase in the higher beta range (26-40Hz) starting around -100ms until 0ms (cluster G), and a relative decrease in the lower beta range (20-25Hz) starting around -50ms until 50ms around the transition (cluster H). The earlier increase in high beta was caused by the young group showing a stronger connectivity increase. The later connectivity decrease was an effect of the older showing stronger coupling in the lower beta range. In the time window after the transition (50 – 260ms), the effect was reversed, i.e., the relative decoupling in the theta/alpha range (5-11Hz) was due to a stronger increase in connectivity in the older participants (cluster I).

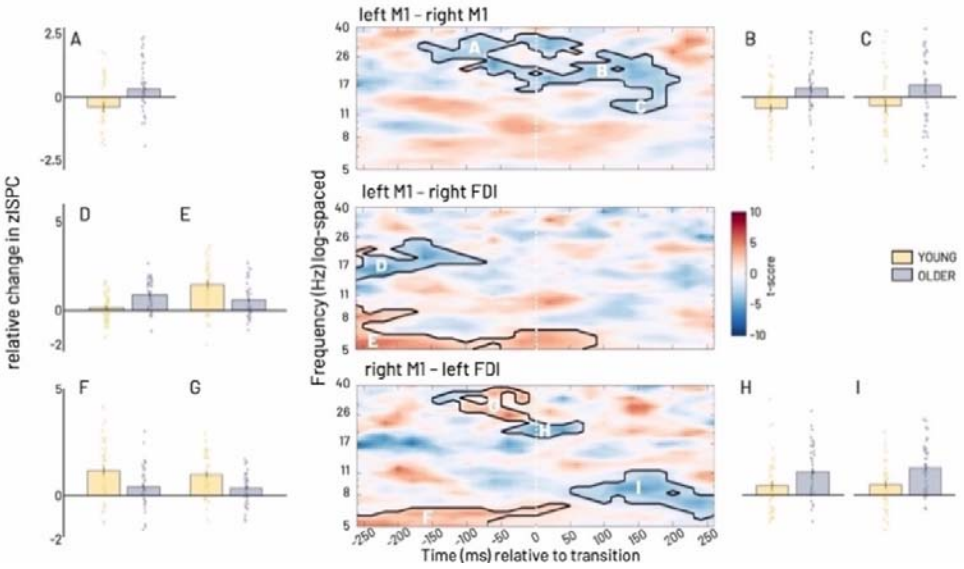

Figure 4 Statistical results of ISPC between left and right M1 source (upper panel), left M1 and right FDI (middle panel), and right M1 and left FDI (lower panel) for group contrast time-locked to the individual mean transition time. *Cluster-corrected z maps for the test of GROUP contrasts [YOUNG –OLDER, t-test against 0, p<.05 2-tailed. Color coding in the time-frequency resolved zISPC plot indicates t-values. Time is plotted relative to individual median transition latency (dashed vertical line at time 0ms). Bar plots indicate group averages of zISPC for respective cluster ranges (white letters in the time-frequency plot correspond to black letters over bar plots), scatter plot depicts individual participants' data within group.*

Condition Contrast [IP – AP]

Left M1 – right M1

For the cortico-cortical connection, a single cluster was visible, extending mostly in the pre-transition time window in the mu to high beta range (Figure 5, upper panel). Between -200 and 0ms, a relative decrease in the full beta range (20-35 Hz) was evident (cluster A). This effect was driven by a decoupling before transitions into IP, while transitions into AP were rather associated with an increase in M1-M1 connectivity before the actual transition was accomplished. Around the time of the transition, -50 – 60ms, a relative increase in connectivity expanded over mu to beta range (cluster B), which was caused by an increased coupling for transitions into IP compared to transitions into AP.

Left M1 – right FDI

The dominant cortico-spinal connection showed several clusters from just before until after the transition across all frequency ranges (Figure 5, middle panel). Around -150 to 0ms relative to the

response, a relative increase in connectivity was visible in the mu to high beta range (15-35Hz). This effect was driven by relatively stronger coupling for transitions into IP (cluster C). After the transition, a relative decrease in connectivity was visible in this frequency range, for which a stronger coupling after transitions into AP was causal (cluster D). Just before the transition a relative increase in connectivity in the theta and low alpha band (5-9Hz) started and lasted until 200ms. A stronger coupling after transitions into IP caused this effect (cluster E). In the higher alpha and mu range (10-14Hz), there was a relative decrease in connectivity after the transition visible (-50-200ms). This effect was caused by a relative connectivity increase for transitions into AP (cluster F).

Right M1 – left FDI

On the non-dominant side, the cortico-spinal connectivity showed several large clusters before and after the transition in mostly all frequency ranges (Figure 5, lower panel). A relative decrease in the theta/low alpha frequency range (5-9Hz) expanded from -200 till 50ms relative to the transition. This effect was driven by more pronounced coupling in transitions into AP (cluster G). In the high alpha / mu range, a relative decrease in connectivity was visible before the transition (-200 - -50ms). Also, in this frequency range, this effect was driven by relatively higher coupling for transitions into AP prior to the transition (cluster H). After the transition, a relative increase in connectivity in the theta/low alpha range (5-9Hz) was evident (50-260ms), which was caused by stronger coupling in transitions into IP (I). After the transition (0 – 260ms), coupling in the high alpha/mu range significantly increased, caused by the transitions into IP and weaker coupling increase for transitions into AP (cluster J). In the beta range, after the transition coupling was relatively decreased in the lower (15-25Hz) and relatively increased in the higher frequency range (>25Hz). The effect in the higher beta range was driven by stronger coupling after transitions into IP (cluster K).

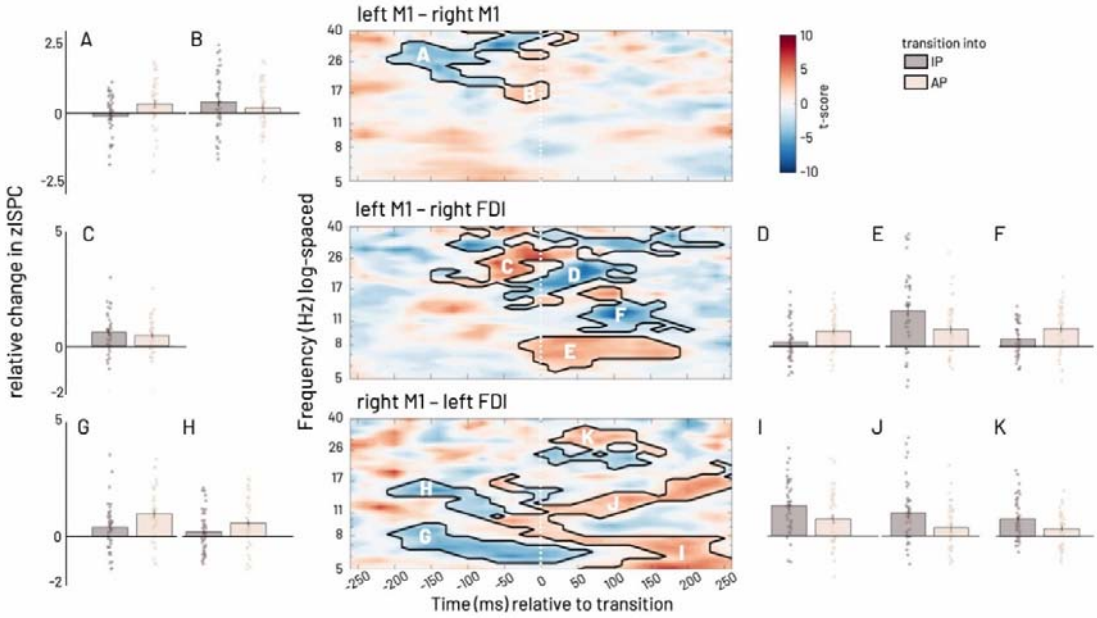

Figure 5 Statistical results of ISPC between left and right M1 source (upper panel), left M1 and right FDI (middle panel), and right M1 and left FDI (lower panel) for condition contrast time-locked to the individual mean transition time. *Cluster-corrected z maps for the test of CONDITION contrasts [IP –AP, t-test against 0, p<.05 2-tailed]. Color coding in the time-frequency resolved zISPC plot indicates t-values. Dashed vertical lines at time 0ms indicate the individual median latency, i.e. the time of response. Bar plots indicate condition averages for respective cluster ranges (white letters in the time-frequency plot correspond to black letters over bar plots), scatter plot depicts individual participants' data per condition.*

Taken together, cortico-cortical as well as cortico-spinal connectivity showed clear age group differences in its spectral features during transitions. Furthermore, while both measures reflected a modulation by task condition (transition into IP versus AP), this effect was stronger and more differentiated in the cortico-spinal coupling. Importantly, we did not find evidence for altered connectivity in the older participants that was specific for transitions into one of the two coordination patterns but rather a general change in connectivity pattern in the older adults.

Association between behavior and connectivity through GABA+

In order to test the impact of baseline GABA+ levels on the relationship between connectivity metrics and behavior in the presence of the effect of age on all three association paths (see Methods for details, schematic model structure given in Figure 1 on the top right), we employed a Bayesian moderated mediation analysis. For this purpose, we modelled the connectivity values extracted from the significant time × frequency sub-clusters of the response-locked analysis (dependent variable), the median transition latency or error rate (dependent variable), the respective GABA+ (mediator), and

age (moderator) and estimated their associations in separate models for each of the individual connectivity pairs. Because all input variables were centered prior to modelling, it is necessary to keep in mind that conditional effects consequently need to be interpreted relative to the respective age group mean. As shown in the results below, for all significant models (see Figure 6a for an overview), age was a relevant effect moderator of all model paths in the case of transition latency (Figure 6b); and to a lesser extent for error rate. Therefore, mediation results are shown conditional on the moderator age, highlighting predominantly opposing trends in the two age groups (regression coefficients for separate model paths given for all Bayesian moderated mediation models in Tables S12-S14).

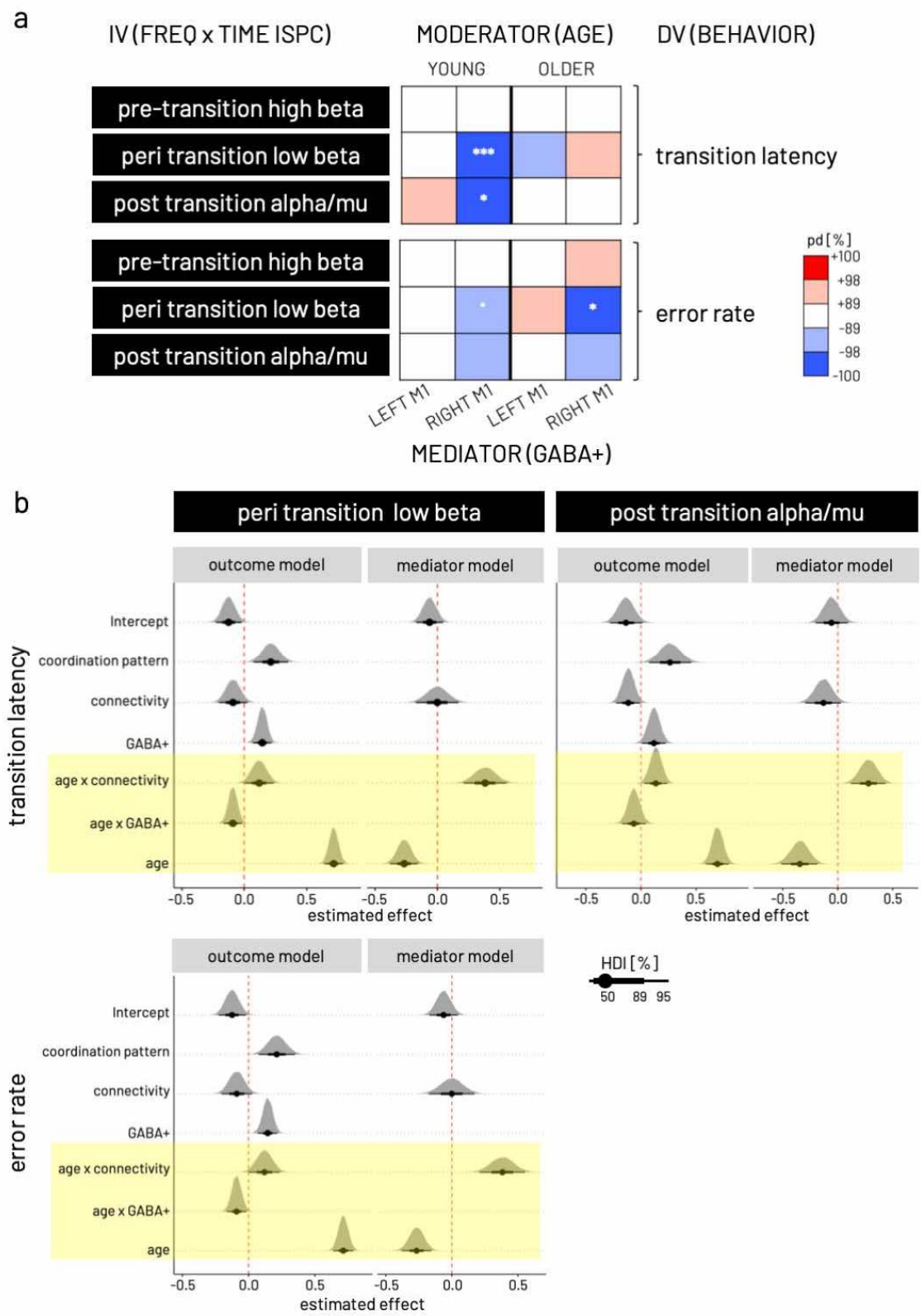

Figure 6 Results of Bayesian moderated mediation analysis for cortico-cortical models. a) *Overview over posterior directions (pd) for indirect effects on transition latency (upper matrix) and error rate (lower matrix) conditional on upper/lower quintiles of moderator age (depicted as YOUNG and OLDER) for the models estimated with the independent*

variable (IV) based on the three time × frequency clusters derived in the response-locked ISPC analysis. For the cortico-cortical models, clusters of group and condition contrasts were overlapping, therefore only group contrasts are depicted. Color coding of pd represents likelihood (in %) and direction of effect, i.e. red shading for positive effects and blue shading for negative effects. A pd of 95, 97.5, 99.5, and 99.95% corresponds to the frequentist 2-sided p-value at the thresholds 0.1˚, 0.05, 0.01**, 0.001*** respectively.* ***b)*** *Probability density plots for effects of parameters in the outcome and the mediator models input to the mediation analysis. Depicted are the three models with significant mediation shown in a). Top row shows outcome models for dependent variable transition latency and peri-transition low beta ISPC (left) as well as post transition alpha/mu ISPC (right). Lower panel shows outcome model for error rate and peri transition low beta ISPC. In all three cases, the mediator model is related to right M1 GABA+. Highlighted in yellow are the significant effects of moderator age in all three models indicated by the posterior distributions of respective parameters falling with >99.5% on one side of the red dashed vertical line. Linewidth of black horizontal bars indicate 50, 89, and 95% highest density interval [HDI] of the parameters' effect.*

Cortico-cortical connectivity significantly predicts behavior in a time and frequency specific manner and this relationship is moderated by age. The main results for the models estimating the association between cortico-cortical connectivity and behavior are graphically summarized in Figure 6a for transition latency and cumulative error rate. In the case of the cortico-cortical models, models including right hemispheric GABA+ levels yielded stronger evidence for mediation effects than those including left hemispheric GABA+ for both age groups. Overall, the young group showed stronger evidence for mediation effects than the older.

Stronger cortico-cortical connectivity makes the young perform better – but not the older. Simulating the total effect, i.e. the association between connectivity and behavior, for the significant models conditional on moderator age reveals the opposing effects within the two groups (age group comparison depicted for one example model in Figure 7a). For all time by frequency clusters, the young participants show strong evidence for a negative association between cortico-cortical connectivity and better behavioral performance, i.e. relatively stronger connectivity is associated with lower (relatively faster) transition time (pd 100%) and with lower error rate (pd >100%, except pre-transition beta). In contrast, within the older adults, relatively stronger cortico-cortical connectivity is associated with a relative slowing in transition latency (pd 100%) but also with a trend for lower error rate (pd >89%, except post-transition alpha/mu).

The young are faster with higher cortico-cortical connectivity in the presence of lower non-dominant GABA+. Simulating the mediation effect conditional on the moderator age, revealed a negative indirect effect of right hemispheric GABA+ (pd >98-100%) on the association between cortico-cortical connectivity on both behavioral outcomes, transition latency and, to a weaker extent (pd >89-95%), on error rate in the young. Specifically, in the presence of lower right M1 GABA+ levels, the negative association between cortico-cortical connectivity in the low beta range during transition [-140:220ms, 15:25 Hz] and transition latency was steeper in the young, i.e. in the presence of low GABA+ levels, stronger connectivity was associated with generally faster transitions while this effect was less pronounced in the presence of high GABA+ levels (Figure 7d). This effect was comparable for cortico-cortical connectivity in the high alpha/mu range post-transition [120:260ms, 12-15Hz] and transition latency (Figure 8a). Importantly, the mediation effect between cortico-cortical connectivity and transition latency was absent in the older for both time x frequency clusters (Figure 7d and 8a). This absence of an indirect effect in the older can be explained by a weak association between the post-transition alpha/mu connectivity and GABA+ (path α) and in particular the absence of an association between GABA+ and transition latency (path β) for both models (depicted for peri-transition low beta in Figure 7b and c).

The older benefit in precision from higher non-dominant GABA+ levels. For the association between cortico-cortical connectivity in the low beta band during transition and error rate, both young (pd >95%) and older (pd >98%) show a negative indirect effect of right M1 GABA+ levels (Figure 6a lower right matrix). Interestingly, this negative mediating effect has diverging consequences on behavior for the two age groups (Figs 8c-d). In the young, again, relatively less cortico-cortical decoupling was associated with better performance, i.e. lower error rate, in the presence of lower non-dominant GABA+, whereas in the older, connectivity variations had a more pronounced impact on the behavior and stronger coupling led to relatively higher error rates in the presence of lower GABA+ levels. In contrast, the association between stronger coupling and worse performance, i.e. higher error rate, was ameliorated in the presence of higher GABA+ levels in the older.

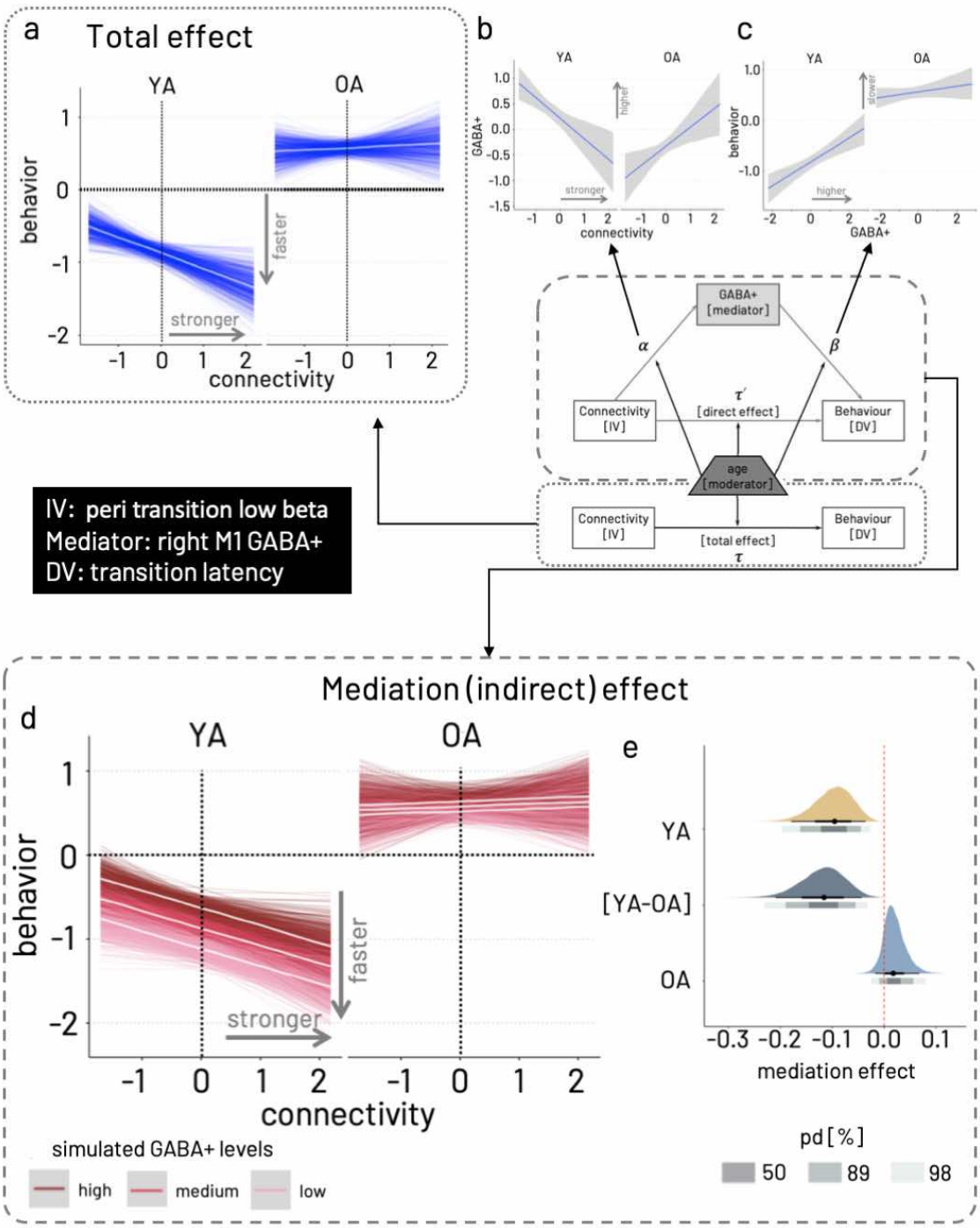

Figure 7 Results of Bayesian moderated mediation analysis for cortico-cortical model for outcome transition latency. a) *The total effect (path τ) conditional on moderator age shows that the YOUNG [YA] generally benefit from stronger M1-M1 connectivity in the beta range, while no association is seen in the OLDER [OA].* ***b)*** *The association between connectivity and GABA+ (path α) shows opposing trends in the two age groups.* ***c)*** *The association between GABA+ and transition latency (path β) is positive in both groups, but the slowing effect with higher GABA+ levels is more pronounced in the young.* ***d)*** *Simulating the mediation effect on the connectivity – behavior association (direct effect, path τ') for varying levels of GABA+ (low – light pink, medium – red, high – dark red), shows that connectivity variations have a stronger impact in the presence of lower GABA+ levels in the YOUNG.* ***e)*** *The negative mediation effect is only present in the YOUNG as depicted in the probability density plot of the indirect effect (yellow) but not the OLDER (blue). The group difference of the mediation effects ([YA-OA] depicted in grey) shows strongly opposing trends between the age groups (pd >98%).*

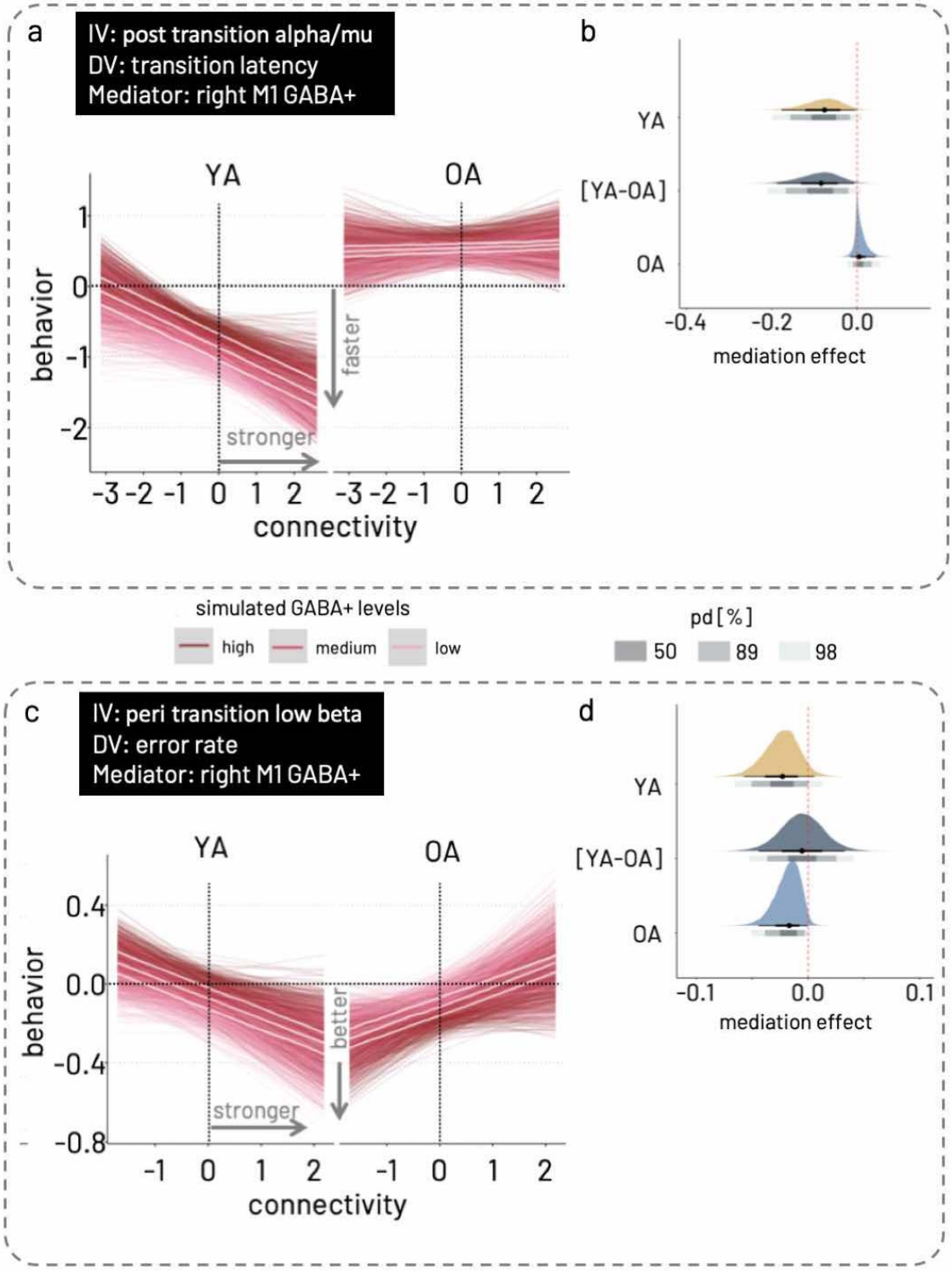

Figure 8 Mediation (indirect) effects of right M1 GABA+ for cortico-cortical models. a) Post-transition high alpha/mu connectivity – transition latency association*. Simulating the mediation effect on the connectivity – behavior association (direct effect, path τ') for varying levels of GABA+ (low – light pink, medium – red, high – dark red) for the association between post-transition mu and transition latency.* ***b)*** *Probability density plot of the indirect effect conditional on age shows a negative indirect effect in the young and no evidence for an indirect effect in the older. The difference plot [YA – OA] shows clear evidence pd >98% for diverging directions of the indirect effects between young and older groups.* ***c) Peri-transition low beta connectivity – error rate association****. Simulations of varying levels of GABA+ reveal opposing trends in*

the two age groups. ***d)*** *Probability density plot of the indirect effect conditional on age for this model shows a negative indirect effect for both age groups.*

No evidence for a mediating effect of GABA+ on cortico-spinal connectivity. When analyzing the indirect effect conditional on the moderator age, only a weak effect (pd >89%) of the left hemispheric GABA+ levels on the relationship between left M1- right FDI and transition latency was found only in the young (Figure 9a left matrix). Cortico-spinal connectivity on the dominant side showed strongly opposing trends of the total effect in all models in the two age groups. While stronger dominant-sided cortico-spinal coherence, irrespective of time and frequency cluster, was associated with relatively faster transition latency in the younger (pd 100%), the opposite was the case in the older. Furthermore, in the young, higher dominant sided cortico-spinal connectivity was only weakly associated with higher error rates (pd >89%). The opposite was the case for the older group, in whom stronger cortico-spinal connectivity across time and frequency clusters was associated with relatively lower error rates (pd >89%).

In the case of the non-dominant side, right hemispheric GABA+ levels showed weak negative effects (all pd >89%) for connectivity between right M1 and left FDI within several time x frequency clusters and transition latency in both age groups (Figure 9b left matrix) and weak positive as well as negative effects (all pd >89%) on error rate on the older only (Figure 9b right matrix). When examining the total effect of non-dominant cortico-spinal connectivity and behavior conditional on the moderator age, stronger connectivity across all time x frequency clusters was associated with faster transition latency in the young (pd >98-100%) and slower transition latency in the older (pd >98-100%, except pre-transition high beta model pd >89%). In the case of error rate, the older showed stronger connectivity, most pronounced in pre-transition high alpha/mu and post-transition theta/low alpha and beta band (pd >98%), to be associated with lower error rate. The young however, showed a more differentiated picture, with stronger pre-transition high alpha/mu connectivity being associated with relatively lower error rates (pd >89% and pd >98%), while stronger post transition beta was associated with relatively higher error rates (pd >89-98%).

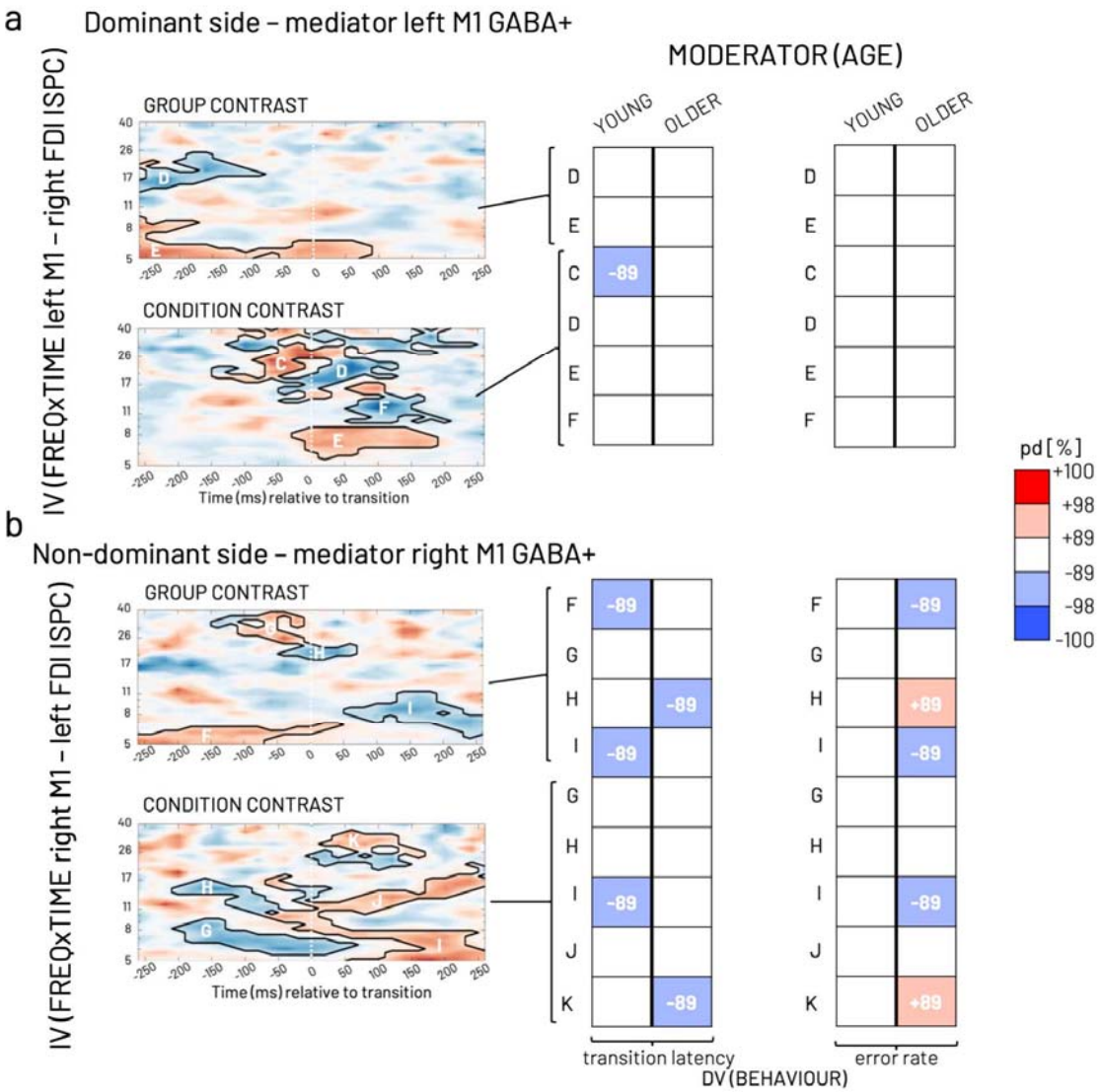

Figure 9 Mediation (indirect) effects estimated for cortico-spinal models. a) Models for dominant side connectivity b) Models for non-dominant side connectivity. *Color coding of pd represents likelihood (in %) and direction of effect, i.e. red shading for positive effects and blue shading for negative effects. A pd of 95, 97.5, 99.5, and 99.95% corresponds to the frequentist 2-sided p-value at the thresholds 0.1, 0.05, 0.01, 0.001 respectively.*

In summary, the multimodal data fusion analysis revealed four main findings with respect to the potential mediating role of baseline GABA+ on the association between connectivity and behavior. First, baseline GABA+ levels exert an indirect effect on the link between cortico-cortical connectivity in the low beta and high alpha/mu frequency band time-locked to the behavioral event and behavior. However, no evidence was found for a mediating role of GABA+ in the cortico-spinal connectivity and behavior association. Second, variations in non-dominant hemispheric (right M1) GABA+ levels were more likely to exert an indirect effect as compared to dominant hemispheric

sensorimotor GABA+ levels. Third, individual variations in baseline GABA+ were found to have a generally more pronounced indirect effect in the young as compared to the older adults. Fourth, the mediating effect of individual variations in baseline GABA+ is of diverging directions in the two age groups: while a state of low GABA+ level benefits the young it seems to be detrimental in the older. Importantly, the latter two points underline the overall expected finding of age being a strong effect moderator for mostly all bimodal relationships investigated here.

Discussion

We used a cross-sectional multimodal approach to test the role of baseline GABA in the brain's responsiveness during behaviorally relevant dynamic neural control mechanisms in the light of healthy aging. Importantly, while the unimodal analyses revealed only marginal age group differences, the multimodal analysis brought to the surface that the direction of the associations between the individual modalities is critically altered by the factor age, which we consider the main finding of the present work. Therefore, we briefly highlight the relevant unimodal findings as a basis for the discussion of the results of the integrated analysis of all three modalities, our main focus.

Age-group differences in neural but not neurochemical and behavioral modality.

From the unimodal analysis steps of GABA+ levels, behavior, as well as cortico-cortical and cortico-spinal connectivity, four key observations are critical prior to discussing the interaction among the three modalities. First, we found a within group anterior-posterior gradient showing higher GABA+ levels in the occipital voxels as compared to both sensorimotor voxels. Although GABA+ levels tended to be lower in sensorimotor voxels in the older, we neither found significant age group differences for the individual voxels nor did we find a significant hemispheric difference within the groups. These findings are in line with the heterogenous picture of MRS-derived GABA findings in aging studies. While the available results in the literature so far point to overall lower GABA concentrations in older adults, irrespective of target area examined, the findings rarely yield large

effect sizes for age group differences in neurotypical and potentially more physically and mentally active volunteers [e.g. [29–33]]. Moreover, age effects seem to partly depend on the reference compound as well as the tissue correction method used because grey matter tissue fraction is one major factor that explains group differences in GABA levels [18, 34], which we controlled for in the measure reported here. A selection bias in favor of a more physically or cognitively active older sample my also distort the existence of an age difference in GABA concentration, which remains a speculative consideration to be confirmed in future work.

Second, older adults were expectedly slower in the motor state transitions [13]. However, the older did neither exhibit more failed transitions, nor a lower number of completely correct transitions. Importantly, we did not find a group difference in the cumulative error rate during motor state transitions. All of these criteria support the assumption that both groups performed at the same qualitative level, which renders our adjustment of the behavioral paradigm with respect to the performance frequency successful. It may also be attributed to the intensive familiarization with the task prior to the experimental session, which favored the strategy of reaching a stable and hence comparable performance level.

Third, the response-locked analysis of cortico-cortical connectivity (left M1-right M1) revealed significant age group differences in the high alpha/mu and the beta frequency range. Specifically, the younger adults showed relative decoupling in both spectral ranges (represented by negative values in Figure 4 upper panel) while the older showed stronger coupling between the primary motor sources, irrespective of transition condition. These results support previous findings of age-related alterations of interhemispheric connectivity in the context of bimanual performance of spatially distinct movements [35]. In spite of task differences, our results agree with the earlier findings of increased interhemispheric coupling in older adults. In contrast to our findings, Loehrer and colleagues found the increased coupling in a broader range that varied with task conditions, i.e. theta to gamma band. In our data, task-condition related modulation of cortico-cortical coupling was also visible in the mu and beta range, however, irrespective of age group. Prior to the transitions, more pronounced decoupling was observed before transitions into IP as compared to transitions into AP.

After the transitions, however, the reversed pattern was visible, i.e. stronger coupling was seen after the transition into IP in contrast to reduced mu- and beta-coupling after transitions into AP. Together, these results suggest that the more complex coordination pattern (AP) required functionally relevant interhemispheric decoupling, which may reflect a role for inhibitory mechanisms to enable the coordination of less congruent bimanual movements, as suggested by previous work [35–37].

Fourth, cortico-spinal connectivity was modulated by age group in the theta/low alpha and the beta range on both, the dominant and the non-dominant side, being time-locked to the transition. In contrast to findings from simple isometric force production [38], the modulation of cortico-muscular synchronization during dynamic motor control in our study engaged frequency ranges below and above the low beta range. Our results support the relevance of theta/low alpha range connectivity, as suggested for dynamic motor action [39]. Since we neglected the gamma range for methodological reasons [40], it is possible that we may have missed task-relevant connectivity modulation, as described for this higher frequency range [41]. The involvement of the higher beta-band connectivity (expanding into the frequency range >30Hz) in young adults on the non-dominant side in the peri-transition time might be taken as an indicator for the additional engagement of gamma band connectivity. Stronger cortico-muscular connectivity in the alpha range has been reported for tasks requiring increased attentional resources [42]. As such, the increase in peri-transition coupling in the theta/alpha frequency range observed here for transitions into both patterns may reflect attentional resource deployment for the given task. Increased cortico-spinal coupling in the theta and alpha range has also been reported in the course of the acquisition of skilled joystick manipulation of a virtual navigation task [43]. It is conceivable that our transition task also required a comparable level of adjustment of cortico-spinal coupling in response to the integration of (visual, sensory, auditory) information and this was possibly specifically controlled in the lower frequency range. Taken together, the unimodal results in part confirm previous work yet highlight the specific sensitivity of phase-based cortico-cortical connectivity to aging-related alterations. In isolation, however, the neurochemical and neural results provide only limited information on their (joint) behavioral relevance.

Specificity of the indirect effect of GABA+ on the cortico-cortical connectivity – behavior relationship.

In order to integrate the three modalities and to investigate the specific role of individual variations in baseline GABA+, we used a Bayesian moderated mediation analysis. We probed the indirect effect of GABA+ on the relationship between phase-based connectivity and behavior for cortico-cortical and cortico-spinal sites with the goal to extract evidence for the specificity of this indirect effect. While fMRI based cortico-cortical connectivity has shown some links to GABAergic signaling [e.g. [11, 44, 45]], cortico-spinal connectivity, on the other hand, is known to depend on inhibitory regulators on spinal level, namely Renshaw cells, and therefore does not solely underlie cortical control mechanisms. Broad-band beta (15-35Hz) cortico-spinal connectivity for example has shown previously to correlate stronger with recurrent inhibition extracted from H-reflexes than with measures of $GABA_A$-mediated synaptic motor-cortical inhibition, as tested with double-pulse transcranial magnetic stimulation [46]. In accordance with this hypothesis, we found no evidence to support a mediating role of GABA+ in the association between dominant or non-dominant M1-FDI connectivity and behavior. Conversely, for the association between cortico-cortical connectivity and behavior, we found a significant indirect effect of right hemispheric GABA+ levels. This effect was specific for the cortico-cortical connectivity in the low beta during and high alpha/mu frequency range after the transition. Most importantly, it revealed marked differences between the two age groups.

Interestingly, the non-dominant sided GABA+ levels yielded higher evidence for an impact on the connectivity-behavior relationship as compared to the dominant side (Figure 6a). Since we used a non-directed measure of connectivity, it is impossible to disentangle the specific contribution of each side to the inter-site communication. Likewise, the behavioral outcome measures used here are measures of synchronized behavior for both hands together rather than each hand's individual performance. It is therefore conceivable that the hemispheric differences of the individual GABA+ levels are the major driver of variance explaining the lateralization in the mediation models of both age groups. It may be that the less well tuned non-dominant sensorimotor system is more susceptible to excitation-inhibition variations and hence has a more pronounced effect on time-sensitive neural

communication. Consistent with this assumption are previous findings of less variance and higher efficiency in sensorimotor processing to co-occur with higher GABA+ levels in the dominant hemisphere [31].

Despite a rather modest age effect in the unimodal analyses outlined above, we found a steep age gradient for the associations between the individual modalities rendering the mediation analysis conditional on the moderator age highly meaningful. Strikingly, while a consistent association between relatively higher connectivity, i.e. less decoupling, in the cortico-cortical connection and better behavioral performance (i.e. faster and fewer errors) was observed in the young adults, no association was seen in the older adults with respect to speed and quite the opposite was evident in the case of error rate (more coupling – more errors, see further). Furthermore, the question emerges how the effect of the mediator baseline GABA+ on the connectivity - behavior association can be explained for the two age groups.

Lower endogenous GABA+ reflects the optimally tuned young neural system.

Compared to the older adults we found overall stronger evidence (pd ≥98%) for a mediating role of baseline GABA+ for the connectivity – behavior relation in the young. Specifically, lower baseline GABA+ in young adults appeared to bring about a stronger effect of connectivity variations on behavior, i.e. in the presence of lower GABA+ levels, relatively less decoupling in the low beta and high alpha/mu range was associated with better performance in terms of speed and precision. This association weakened in the presence of higher GABA+ levels.

Computational modeling supports that extra-cellular GABA levels, as most likely primarily detected with MRS [47, 48], are critically influencing the variability in cortical neural activity and thereby define adequate information processing and integration [49]. Individual variations of regionally-specific GABA levels, investigated with MRS, have been found to predict performance in a range of perceptual modalities [50, 51] and in the motor domain [52] in humans. But why may relatively lower GABA levels be behaviorally more beneficial in young adults for the present task? One possible explanation may be that the young's well-tuned neural system can afford it and low

extracellular GABA+ concentration represents the physiological environment with the optimal inhibitory tone for efficient and timely precise up- and down-regulation of phasic synaptic inhibition [53]. In support of this concept, previous pharmacological work has shown that increases beyond the physiological GABA+ concentration has detrimental effects on neural processing that co-occurs with negative effects on perception and behavior in young healthy volunteers. Hereof, perceptual processing has been shown susceptible to pharmacologically increasing endogenous GABA beyond physiological levels, as evidenced by exaggerating amplitudes of early evoked responses in the somatosensory cortical areas [54] and decreasing amplitudes of medium-latency evoked responses in the visual cortex [55]. These drug-induced changes of evoked responses have been hypothesized to indicate at least two distinct mechanisms in neural processing that are vulnerable to increasing inhibition, namely a potential disturbance of refractory mechanisms leading to hyperpolarization [54] and an alteration of the excitatory drive [55]. Previous findings showing that elevated GABA concentration affects pyramidal and inter-neuronal cell populations and exerts effects on both phasic and tonic inhibitory signaling in superficial and deep cortical layers serve as a potential explanation [56–58]. Simply speaking, too much inhibition may turn into overall excitation. In other words, because of the interdependence of tonic and phasic inhibitory mechanisms, acutely increased inhibitory tone may lead to a reduction of phasic inhibition and thus promote excitation [59]. It is worth noting that lowering GABAergic concentration below physiological levels, on the other hand, also has shown to cause acute disturbance of spontaneous neural activity and perceptual processing in the primary visual cortex in young macaque monkeys [60, 61]. Therefore, the available findings may best be summed up as evidence for the delicate equilibrium between excitation and inhibition in the young's neural system, which assures dynamic neural processing in a given (task-related) context.

Support for this hypothesis comes from the domain of sensorimotor control, in which a pharmacologically increased GABAergic drive has been specifically linked to strengthened movement-related desynchronization in the beta-frequency range detected over the primary motor cortex [62]. This former work has shown that, in contrast to peri-movement gamma-band synchronization or post-movement beta-band synchronization, the amount of amplitude reduction

(desynchronization) in sensorimotor beta-band oscillations was critically susceptible to pharmacological manipulation with benzodiazepine. These former findings are well in line with the present frequency-band specificity of the mediating effect of GABA levels, as found here in the young. That is to say, the indirect effect of GABA was specific to the association between the fine-tuning of task-related decoupling in the mu- and low beta-band during the motor state transitions and larger efficiency of behavior. In the present sample, relatively lower endogenous GABA levels in the young might, therefore, reflect the young neural system's general readiness for the effective neural communication in response to the dynamic task requirements.

Higher GABA+ indicates neural system integrity and better functioning in the older.

In older adults, evidence for the mediation effect of GABA+ was generally absent or weak with one exception, i.e. the association between peri-transition connectivity in the low beta range and error rate. As opposed to the findings in the young, the effect of baseline GABA+ appeared to be of opposite direction, i.e. higher GABA+ levels ameliorated the association between higher connectivity, i.e. stronger synchronization in the low beta frequency band and error rates. In other words, older adults performed less erroneous with higher beta-band connectivity in the presence of higher GABA+ levels.

The question is as to why the older do not benefit from the relatively lower GABA+ levels in the same way the younger adults do? To answer this question, it is necessary to reflect on the nature of the age-related behavioral decline. Our observation of older adults showing no group difference in overall error rate and a higher number of fully correct transitions, could be interpreted as a sign for a strategic difference, i.e. older prioritizing precision over speed. Following this assumption, the observation may be explained as a behavioral read-out for the speed-accuracy trade-off in the older based on an active choice "to play safe" (i.e., increase accuracy) at the cost of slower performance [63]. The question remains why this strategy to slow down is necessary in the first place. Alternatively, age-related deterioration in neural processing speed in addition to lower signal-to-noise ratio of neural processing may serve as explanations for the effect of variations in GABA levels in

older adults. Following this alternative assumption, higher GABA+ concentration has been suggested to promote lower errors through optimal tuning of neural activity (reduced variability), promoting a better signal-to-noise ratio in the older. One effect of higher signal-to-noise is a more efficient perceptual filtering function from lower to higher level processing stages. A growing body of results from animal models [e.g. [60, 61]], computational modeling [49, 64], as well as results from aging human volunteers [e.g. [33]] supports this hypothesis. Neural conduction time, on the other hand, depends to a greater extent on other factors, such as for example axon diameter or myelination. Therefore, it is not or to a lesser extent influenced by varying GABA levels. From this perspective, the mediating effect of GABA levels on the association between beta-band connectivity during the behavioral transition and error rate but not performance speed in older adults appears conceivable.

Individual variations of endogenous GABA levels may also impact differently on the connectivity – behavior relationship when the system is overall in a state of stronger coupling as seen here in the older. It is important to keep in mind that the cortico-cortical connectivity in the present study was modulated on a level of overall increased coupling in the older, whereas in the young a relative decoupling was observed throughout the motor-state transitions. In this regard, reduced endogenous GABA+ levels have been linked to decreased resting-state network segregation, i.e. increased connectivity, and lower sensorimotor performance in older adults, impacting general functionality [11]. Although controversial findings exist, an increased interregional coupling has frequently been observed across imaging methods in older populations during task-free [65, 66] and task-related conditions [67, 68] supporting the hypothesis of age-related dedifferentiation. The question as to whether alterations in GABAergic transmission reflect the cause or the 'cure' (i.e. compensation) for age-related neuronal functional decline reflected in behavioral performance deficits, remains to be answered. We suggest that it is well possible that age-related functional decline is accompanied by a non-linear trajectory of changes to the GABAergic inhibitory system, which develops on a continuum from compensatory to detrimental effects. Consequently, the increased GABA+ level may be beneficial in a certain stage of healthy aging but this effect may wear out with increasing age.

In view of the limitations of the present work, it is necessary to point out that strictly speaking, a mediation implies the assumption of causality, which was not upheld in the present cross-sectional study. We believe, however, that our results may inspire further hypothesis-testing studies, ideally with larger sample sizes. Considering the collision or confound of many other factors modifying age-related changes of the brain-behavior interaction neglected here, our findings highlight the importance to investigate the nature of the interactions as a function of age. Finally, our Bayesian moderated mediation analysis, though hypothesis-driven, followed an exploratory approach and we acknowledge the lack of a cross-validation. This shortcoming should be addressed in future work.

Conclusion

The present work suggests that endogenous GABA concentration may carry a critical role as mediator of brain-behavior interactions, which is specific to cortico-cortical connections. This mediating role changes during the course of healthy aging and potentially underlies hemispheric differences. While we found relatively lower GABA to be more beneficial for the association between cortico-cortical connectivity and behavior in the young, the older showed a beneficial behavioral effect in the presence of higher GABA concentration given their generally elevated task-related connectivity. This age-related alteration of the preferred state of endogenous GABA concentration may reflect a compensatory mechanism, allowing for higher temporal precision in neural tuning and preservation of a higher level of behavioral functioning. The present findings provide essential groundwork to causally probe the neurochemical – neural – behavioral framework to target age-related cognitive decline.

Materials and Methods

Ethics Statement

The protocol and all procedures of this study complied with the ethical requirements in accordance with the Declaration of Helsinki in its revised version from 2008, as approved by the medical ethical

committee of the KU Leuven (local protocol number S-58811, Belgian registration number B322201628182). All participants gave written informed consent to all of the study's experimental procedures and were reimbursed with 15 € per hour.

Participants

44 volunteers (older group N = 22, age range 62-82 years of age; young group N = 22, age range 21 – 27 years of age) were recruited through local advertisements and were screened for in- and exclusion criteria. One young participant dropped out after the MRI data acquisition for personal reasons unrelated to the study. MRI, EEG, and behavioral data were thus collected in 21 young (10 women) and 22 older (11 women) participants. All participants were right-handed, as evaluated with Edinburgh Handedness Inventory [69] (laterality quotient: older 92.50±0.20, young 85.00±0.15, median±95% CI). All participants were free from neurological impairments and musculoskeletal diseases affecting the unconstrained movement of the fingers, did not take neuroactive drugs, and had normal or corrected-to-normal vision as evaluated with an in-house standardized questionnaire.

Magnetic Resonance Imaging (MRI) and Magnetic Resonance Spectroscopy (MRS) acquisition

A 3D high-resolution T1-weighted structural image (repetition time = 9.5 ms; echo time = 4.6 ms; voxel size = 0.98 x 0.98 x 1.2 mm^3; field of view = 250 x 250 x 222 mm^3; 185 coronal slices) was acquired for each participant using a Philips Achieva 3.0T MRI system and a 32-channel head coil. The 30x30x30mm^3 MRS voxels were positioned based on the T1-weighted image. For the left and right sensorimotor voxels, this was centered above the hand knob area [70] and rotated in the coronal and sagittal planes to align with the cortical surface of the brain. The occipital voxel was medially centered over the interhemispheric fissure, with the inferior boundary of the voxel aligned in parallel to the Tentorium cerebelli to cover left and right occipital lobes symmetrically [71].

Data were acquired using the Mescher–Garwood point resolved spectroscopy (MEGA-PRESS) sequence [72], with parameters resembling those of previous work [16–18]; 14ms sinc-Gaussian

editing pulses applied at an offset of 1.9 ppm in the ON experiment and 7.46 ppm in the OFF experiment, TR = 2000ms, TE = 68ms, 2000 Hz spectral bandwidth, MOIST water suppression, 320 averages, scan duration of 11 minutes, 12 seconds]. Sixteen water-unsuppressed averages were acquired from the same voxel. These scan parameters were identical for all three voxels.

MRS data were analyzed with the Gannet software 3.0 toolkit [73]. Individual frequency domain spectra were frequency- and phase-corrected using spectral registration [74] and filtered with a 3Hz exponential line broadening. Individual ON and OFF spectra were averaged and subtracted, yielding an edited difference spectrum, which was modelled at 3ppm with a single Gaussian peak and a 5-parameter Gaussian model. The unsuppressed water signal serving as the reference compound [75], was fit with a Gaussian-Lorentzian model. The integrals of the modelled data were then used to quantify the uncorrected GABA levels. As discussed extensively, this method edits GABA as well as macromolecules at 3 ppm [76, 77], therefore GABA levels reported are referred to as GABA+ (i.e., GABA+ macromolecules). To adjust GABA+ levels for heterogeneity in voxel tissue composition, MRS voxels co-registered to the high-resolution anatomical image were segmented into three different tissue classes namely gray matter (GM), white matter (WM), and cerebrospinal fluid (CSF) with SPM 12 (http://www.fil.ion.ucl.ac.uk/spm/software/spm12/). The resulting voxel compositions were used to extract tissue-corrected GABA+ following the assumptions that GABA+ levels are negligible in CSF and twice as high in GM relative to WM [78], accounting for tissue-specific relaxation and water visibility values [78]. GABA+ levels were normalized to the average voxel composition within each age group after outlier removal [78]. Quality of the MRS data was assessed using the quantitative metrics GABA and the N-acetylaspartate signal-to-noise ratio (GABA_SNR, NAA_SNR), fit error of the GABA peak (GABA_FitError), the drift (Drift) and the standard deviation of the water frequency offset (FreqOffset), as well as linewidth, quantified as the full-width half-maximum of the modelled and N-acetylaspartate (NAA_FWHM) signal.

Behavioral Paradigm

The behavioral task involved two coordination patterns representing the two motor states, i.e. a mirror-symmetric synchronous tapping of homologue fingers (in-phase, IP, the more stable motor state) and a synchronous tapping of the index and middle finger of opposite hands (anti-phase, AP, the less stable motor state). Since the AP coordination pattern has been shown to represent the coordinatively more challenging pattern [12, 19, 79], tapping frequency was individually adjusted to 80% of the frequency with which the AP pattern was comfortably performed without involuntary spontaneous transitions into the IP coordination pattern. This individual tapping frequency was auditory paced throughout the complete experiment. During the EEG session, the auditory pacing stimulus was provided through insert etymotic earphones with flat frequency response (Cortech Solutions, Wilmington, NC, USA). Tapping was performed on a custom-made keyboard with six input keys (1000Hz sampling rate). Visual target cues were presented on a standard 19" computer screen (refresh rate 60Hz) and indicated which movement pattern to perform. Visual and auditory stimuli of the behavioral paradigm were programmed in LabVIEW 2016 (National Instruments, Austin/TX, USA). One complete trial consisted of a start cue subsequently followed by a cue to either continue with the same coordination pattern ('continuation') or transition into the respective other pattern ('switching' from IP to AP, or vice versa, Figure 1a). The main focus was set on the switching transitions, which were selected for EEG analysis (see below for details). To yield a maximum trial count for the EEG analysis, the ratio of occurrence of continuation versus switching transitions was set to approximately 1:5. Trials were interleaved with pauses ('pause'), which were always of the same length (3000ms); the other events had a jittered inter-stimulus interval (5000-8000ms). In order to preserve attention at a high level throughout the experiment, an additional thumb reaction time task (tRT) was included, which could occur instead of any other event type with a chance of 5%. The instruction was to respond as fast as possible upon cue occurrence (a magenta circle on left or right side of fixation cross) indicating either the left or right thumb to press the respective key. The tRT task was always followed by a pause with a latency of 1000ms to avoid interference with continuation/switching transition performance. In order to minimize eye movements, participants

were instructed to fixate a small cross in the center of the screen, which was visible at all times, during and in-between all cue presentations. For the within-trial pauses ('pause'), the instruction was to further attend to the fixation cross with minimal movement of the fingers or other body parts because these phases served as baseline for the EEG data analysis. Stimulus-response mapping was acquired during a training session held one day prior to the experiment. In this training session, a general familiarization with the keyboard was followed by the standardized frequency adjustment procedure. Subsequently, the visual cues were introduced with a visual presentation after which on average 44±21 minutes (young: 36±16min., older: 51±23min.) of training were performed in the individual tapping frequency until the participants were able to successfully perform one block of 14 trials. In the main experiment, the individual tapping frequency was re-adjusted and the participants performed in total 12 blocks of on average 14 trials each. Each block had a duration of approximately 4 minutes. Participants were given short breaks of individual length between each block in order to rest the eyes and make small movements.

EEG and EMG recording and pre-processing

Continuous EEG was recorded from 127 cephalic active surface electrodes (actiCAP, BrainProducts GmbH, Gilching/Germany) arranged according to the 10-10 system and referenced to the FCz electrode (implicit reference). Scalp-electrode impedance was kept below 20kΩ. Data were acquired with a sampling rate of 1kHz (BrainVision Recorder, version 1.21.0004, BrainProducts GmbH, Gilching/Germany).

Electrooculogram (EOG) was recorded using bipolar channels. For the EOG, silver/silver-chloride cup electrodes were placed on the left and right zygomatic processes (horizontal EOG) and on the left supraorbital process as well as on the sphenoid bone below the eye (vertical EOG). Electromyogram (EMG) was recorded using a bipolar muscle-tendon montage with pairs of adhesive electrodes placed approximately 5 cm apart over the belly and tendon of left and right first dorsal interosseous (FDI), flexor digitorum superficialis (FDS), and extensor digitorum communis (EDC) muscles. A separate ground electrode for the EMG was placed over the right processus styloideus ulnae. EEG and EMG

were recorded with a high cut-off at 280Hz. Voltage resolution for EEG and EMG channels was set at 0.1μV and 0.5μV, respectively.

All EEG and EMG data (pre-) processing and analyses were performed using functions from the EEGLAB toolbox version 2019.0 [80], the Fieldtrip toolbox version 20190419 [81], and customised Matlab functions (Matlab 2018b, MathWorks, Natick, MA, USA).

Off-line, data from EEG channels were high-pass filtered with a 1Hz cut-off to remove baseline drift and down-sampled to 250Hz. Line noise at 50 and 100Hz was removed based on a frequency-domain (multi-taper) regression with the 'pop_cleanline' function of EEGLAB. Subsequently, continuous data were segmented into epochs of 5 seconds length, ±2.5 seconds around the "start" (baseline) and the "transition" (time of interest) events in order to limit the effect of edge artifacts (Figure 1b).

Thereafter, a rigorous artefact removal pipeline was employed to minimize the effect of high muscle-related artefact while ensuring sufficient data for subsequent analyses. This procedure included a combination of semi-automatic and visual inspection steps. First, bad channels were identified and removed (EEGLAB trimOutlier plugin with 2μV as lower and 100μV as higher cut-off for identification of bad channels). Then canonical correlation analysis (implemented in the EEGLAB AAR plugin) [82] was used to identify and remove excessive EMG activity present in the data due to the motor task (288 seconds window length and shift between correlative analysis windows, 10^6 eigenratio, 15Hz, ratio of 10, based on the welch algorithm). Thereafter, independent component analysis (runica/Infomax algorithm as implemented in EEGLAB) and SASICA was used as a semi-automatic procedure to inform removal of eye-movement -related and residual muscle artefacts [83]. For the identification of ICs representing relevant artifacts, MARA, FASTER, and ADJUST algorithms were used, and components were rejected if they contributed ≥4% of the total data variance. Epochs with remaining muscle artefacts were removed based on trial-by-trial visual inspection. On average 50 trials per condition/participant went into further analysis. As a final step, available EEG channels were re-referenced to a common average reference.

Data from EMG channels were high-pass filtered at 5Hz and not rectified [84], line noise and its harmonics (50, 100, and 150Hz) were removed (EEGLAB function pop_cleanline). The EMG amplitude was then estimated with the absolute value of the Hilbert-transformed signal using the Matlab function 'hilbert' [85, 86], down-sampled to 250Hz, and appended with source time series data (computation detailed in following section) by matching the valid EEG epochs to the respective EMG time windows. As a result of the described preprocessing, on average 53.9±4.8 (52.7±5.7 older, 55.1±3.2 young) trials per transition condition/participant were entered into the subsequent analysis steps.

Localisation of neuronal sources

For the forward solution, an individual head model was created for each participant based on the same high-resolution structural MR image as used for the MRS analysis and 3D locations of the electrodes, registered with an optical infrared-camera based (NDI, Ontario, Canada) neuronavigation system (xensor™, ANT Neuro, Enschede, Netherlands). For the individual geometrical description of the head (mesh), the anatomical image was segmented into 12 tissue classes (skin, eyes, muscle, fat, spongy bone, compact bone, cortical gray matter, cerebellar gray matter, cortical white matter, cerebellar white matter, cerebrospinal fluid and brain stem), based on the MIMA model [87] using SPM12 (http://www.fil.ion.ucl.ac.uk/spm/software/spm12/) as described previously [88–90]. The EEG electrode positions were rigidly co-registered to the individual head surface (skin contour) by projecting the electrode coordinates in the native space through a rigid-body transformation, based on: (i) the estimation of anatomical landmarks (nasion, left/right peri-auricular points), (ii) the alignment of the electrode positions on the head surface through Iterative-Closest Point registration, and (iii) the projection of the electrodes onto the surface choosing the smallest Euclidean distance [91]. Conductivity values for each tissue class were grounded on previous findings [92, 93]. Dipole sources were constrained by a regularly spaced 6mm three-dimensional grid spanning both the cortical/subcortical and the cerebellar gray matter. The volume conductor model was constructed based on a whole-head finite element model [94] using the SimBio toolbox (https://www.mrt.uni-

jena.de/simbio) implemented in FieldTrip. In order to solve the inverse problem of describing the source activity, we made use of exact low-resolution brain electromagnetic tomography (eLoreta) algorithm [95], using a regularization factor $\lambda = .05$.

Source space time series were reconstructed using the precomputed filter for three regions of interest, the left and right primary motor cortex and the occipital cortex. Coordinates for these regions of interest were extracted from the group (OLDER vs. YOUNG) averages of the individual centroid coordinates of the MRS voxels in MNI space and transformed into native space. We used a sphere with a 6mm radius around the coordinates as a search grid to retrieve the gray matter grid voxel with the shortest distance to the coordinates of interest. Subsequently, singular value decomposition was used to reduce the dimensionality of the source activity time series in the target voxel from the x-, y- and z-components of the equivalent current dipole source to the projection that carried the maximal signal variance, i.e. the largest (temporal) eigenvector.

Cortico-spinal and cortico-cortical connectivity

In order to study the connectivity between cortical sources and muscles as a function of time, wavelet-based inter-site phase clustering, ISPC [96] was used. This phase-based connectivity measure depends on the distribution of the phase angle differences of two signals in polar space. The underlying assumption is that two neural sources are functionally coupled when their oscillations show temporal synchronization evidenced by angular differences. ISPC is a non-directional measure.

In order to extract the phase angles, spectral decomposition was computed by convolving the ROI source signal with a set of complex Morlet wavelets, defined as complex sine waves tapered by a Gaussian [97]. The frequencies of the wavelets were chosen from 2 Hz to 40 Hz in 50 logarithmically spaced steps in order to retrieve the full theta to beta frequency range. The full-width half-maximum (FWHM) ranged from 400 to 104ms with increasing wavelet peak frequency, corresponding to a spectral FWHM varying between 1.5 Hz and 12 Hz [98]. Subsequently, ISPC was computed for 35 frequency steps from 5:40 Hz in order to cover the frequency range available in the EMG signal.

The phase angle differences were computed between ROI source and EMG signals over time and averaged over task conditions [96, 99] on the down-sampled data (50Hz) following

Eq.1 $$ISPC_f = \left| n^{-1} \sum_{t=1}^{n} e^{i(\phi_{xt} - \phi_{yt})} \right|$$

where n is the number of time points, and ϕ_x and ϕ_y are phase angles from signals x and y at frequency f. Temporal modulation of ISPC change was evaluated in the time of interest (0 to +2000 post-cue, Figure 1b) relative to the baseline period (-500 to -200ms) computed by subtracting the baseline ISPC values from the ISPC values in the time of interest.

Additionally, instantaneous power was calculated by squaring the complex convolution results. Power spectra were normalized by converting the values to dB change relative to the fused within-trial baseline period, which was generated by averaging the time window between -500 and -200ms before the cue over all start trials [100].

Statistical analysis

The statistical analysis involved in a first step the analysis of the individual outcome modalities (MRS, behavior, and EEG) and in a second step the joined analysis of all three outcome modalities.

Generally, for all generalized linear mixed effects models (GLMM) described in the following, the goodness of fit was visually inspected based on the distribution of residuals. Models were fitted with a random intercept on subject level after validating that this improved model fit compared to the fixed effects model. Model comparison was performed based on Akaike Information Criterion (AIC) and Bayesian Information Criterion (BIC). Parameter estimates for fixed effects and their interactions as well as 95% Confidence Intervals (CIs) and p-values were computed using Wald approximation. Parameter estimates for logistic models are reported as logits, i.e. log odds, as well as odds ratios. In the case of the beta model with logit link, parameter estimates are reported as proportions and change in rate of proportion. Standardized parameters were obtained by fitting the model on a standardized version of the dataset. Relevant interactions were followed up with contrasts for model estimated marginal means of parameter levels and reported as standardized differences (ΔEMM±standard error,

95% CI, z-value p-value FDR-adjusted for multiple comparisons). Effect sizes are reported for the models' total explanatory power with conditional R^2 and for the fixed effects part alone with marginal R^2 [101, 102]. Forest plots are used to given an overview over the models' parameter estimates with CI, direction, and significance of their effects. Distribution and boxplots are used to represent summary statistics of group data. Computed variables for boxplots: lower/upper whiskers represent smallest/largest observation greater than or equal to lower hinge ± 1.5 * inter- quartile range (IQR), lower/upper hinge reflects 25%/75% quantile, lower edge of notch = median − 1.58 * IQR/ sqrt(n), middle of notch reflects group median.

Analysis of the MRS data

GABA+ data were best estimated with a GLMM showing optimized fit modelling a gamma distribution and identity link function. Factors GROUP, VOXEL, and their interaction were modelled as fixed effects based on the study design variables. Random intercepts were fit on subject level. In order to identify the influence of the quality metrics and their potential interaction with group or voxel, a stepwise backwards selection approach was taken starting from a beyond optimal model with all quantitative quality metrics and their interaction with voxel and group modelled as fixed effects. Based on the significance of parameters estimates, non-significant interactions were eliminated.

Analysis of the behavioral data

Error rate. To analyze the occurrence of errors within the behavioral task, we chose to code and analyze three different aspects of the error information in the data in order to account for the skewed distribution of percentage data and the inherently zero-inflated data.

First, the data was transformed in a binary outcome coding *failed transitions*, i.e. trials with an error rate of 100%. Binarization of the data was achieved by coding fully erroneous trials as "1" and all other trials as "0". This step was done based on the full set of available trials. A GLMM was used as a hurdle model and fit to the data with a Poisson distribution and logit link.

Second, after removing the fully erroneous trials, the remaining data was transformed in a binary outcome coding *fully correct transitions*, i.e. an error rate of 0 coded as "1", versus erroneous trials,

i.e. and error rate >0 coded as “0”. As described in the first step, a GLMM was used as a hurdle model and fit to the data with a Poisson distribution and logit link.

Third, *cumulative error rate* in the trials not considered fully correct or fully erroneous, i.e. non-zero-inflated trials, were transformed into the range of the beta distribution [0<error rate/100<1] and modelled as such using a GLMM with a “logit” link function. Factors GROUP (old, young), COORDINATION PATTERN (IP, AP), TRANSITION CONDITION (continuation, switching), and covariate nTRIALc (trial number, centered) were entered as fixed effects. Random intercepts were modelled on subject level.

Transition Latency. Transition latency did not follow a normal distribution and was therefore analyzed with a GLMM showing optimized fit assuming a gamma distribution and log link function. Factors GROUP (old, young), COORDINATION PATTERN (IP, AP), TRANSITION CONDITION (continuation, switching), and covariate nTRIALc (trial number, centered) were entered as fixed effects. Random intercepts were modelled on subject level.

The additional thumb reaction time task (tRT) was analyzed separately; methods and results are reported in Table S8.

Analysis of the EEG data

EEG/EMG data were analyzed with the main focus on phase-related connectivity (ISPC) between motor-cortical source and the signal from intrinsic hand muscles. The statistical analysis of the task-related modulation of the spectral signature followed the pipeline described for ISPC below. Additional methods and results are presented in Figures S9 and S10 to allow the interpretation of the association/independence of ISPC and spectral power changes.

The effect of task condition and age group on the frequency-band specific modulation of connectivity (inter-site phase clustering, ISPC) was analyzed in three steps. First, ISPC change from baseline was analyzed within subject using a cluster corrected permutation (1000 permutations, 2-tailed t-test, $p<.05$) to extract the effect size of change from baseline irrespective of task condition. This step was

used to extract the z-transformed ISPC changes (zISPC) per condition within subject. In this and the subsequent steps, clusters were corrected for multiple comparisons and considered significant if they contained more time × frequency data points than expected under the null hypothesis at $p<.05$ [103].

Second, group-level cluster-based permutation analysis (1000 permutations, 2-tailed t-test, $p<.05$) of change in baseline-subtracted zISPC pooled over task conditions (stimulus-locked analysis) was used to confirm the relevance of connectivity modulation within the selected time and frequency windows. The results of this second step containing the stimulus-locked analysis of connectivity modulation are presented in Figure S11.

Third, in order to test the effect task condition and its modulation by age group, differences of the z matrices were calculated for the task condition contrast (IP – AP) for the age groups separately and subsequently subtracted from each other ([IP-AP]YOUNG – [IP-AP]OLDER). A two-sided t-test ($p<.05$) was then run with permuting the age group allocation (1000 permutations).

The third step was performed relative to the response, i.e. ±260ms around the individual median transition latency specific for IP and AP transitions, respectively (response-locked analysis). As task-related connectivity was not modulated by an interaction of condition and age group; therefore, both factors were tested subsequently in separate t-tests permuting the respective factor level allocation (1000 permutations, $p<.05$).

Analysis of the association between connectivity and behavior through GABA+

The next goal was to get further insight into the relationship between EEG-derived connectivity metrics and behavior and the potential impact of endogenous GABA+ levels on this relationship in the presence of the effect of age. Therefore, we made use of Bayesian moderated mediation analysis modelling GABA+ as mediator and age as moderator variable and their impact on the relationship between cortico-cortical and cortico-spinal connectivity and behavior, i.e. *transition latency* and *error rate* (including *cumulative error rate* and fully *correct transitions* but excluding *failed transitions*). This approach allowed us to further dissect the connectivity – behavior relationship given the individual variations of background GABA+ levels in the context of assumed aging-related changes of the associations between all variables. The Bayesian approach permits accounting for the non-

gaussian data structure of the present sample and its size [104]. Conceptually, a moderated mediation model is built based on two regression models, in this case two generalized linear models, one that estimates the effect of the independent variables and relevant covariates (here the moderator) on the dependent variable (the outcome model, Eq. 2), and the second, which estimates the effect of the independent variable and relevant covariates on the mediator (the mediator model, Eq. 3):

Eq. 2 $Y = i_1 + c_1X + c_2W + c_3XW + b_1M + b_2MW + e_1$

Eq. 3 $M = i_2 + a_1X + a_2W + a_3XW + e_2$.

In these models, $i_1$and i_2 are intercepts, Y is the dependent variable, X is the independent variable, M is the mediator, and W is the moderator W interacting with each variable. In the outcome model (Eq. 2), $c1$ is the coefficient relating the independent variable and the dependent variable, b_1 is the coefficient relating the moderator to the dependent variable, c_2 identifies the coefficient relating moderator and independent variable, the coefficients for the interactions with the moderator are c_3 and b_2. In the mediator model (E. 3.), a_1 is the coefficient relating the independent variable with the mediator, a_2 is the coefficient relating the moderator with the mediator, and a_3 is the coefficient for the interaction of the independent variable and the moderator. The residuals are identified by e_1 and e_2. These two models are combined within one multilevel model and estimated simultaneously for the moderated mediation analysis.

Here, a series of individual moderated mediation models was run for each connectivity pair (left M1-right M1, left M1 – right FDI, right M1 – left FDI), using the respective zISPC pooled over the significant time × frequency clusters in addition to the GABA+ values of the corresponding voxel (e.g. model 1: predictor variable left M1 – right M1 zISPC, outcome variable transition latency, mediator variable left M1 GABA+, model 2: predictor variable left M1 – right M1 zISPC, outcome variable transition latency, mediator variable right M1 GABA+). Coordination pattern (IP vs. AP) was included in the outcome model to account for its significant impact on both behavior and connectivity. Within each moderated mediation model, different associations (model paths) moderated by age were jointly estimated: i) the association between independent and dependent variable in the absence of mediation (path τ, total effect); ii) the association between independent variable and mediator (path

α); iii) the association between mediator and dependent variable (path β); iii) the mediation effect (α*β, indirect effect); and iv) the association between independent and dependent variable after adjusting for mediation (path τ', direct effect) [104]. A schematic of the moderated mediation model framework is given in the inlay in Figure 1a on the top right.

All input variables were centered prior to fitting the GLMMs for outcome and mediator models using an exgaussian distribution, identity link functions (for mu, sigma, and beta), and uniform priors. Posterior distributions for multivariate models were obtained using Hamiltonian Monte-Carlo algorithm using Stan [105] implemented for R with brms [106, 107] and rstanarm [108] packages. Four random walk chains each with 10.000 iterations discarding the first 1000 iterations (burn-in) were used for inference. Model convergence was examined using pareto-k diagnostics, approximate leave-one-out criterium (LOO), R-hat, and effective sample size (bulk-/tail-ESS); Bayesian R^2 served as indicator for quality of model fit. Median estimates and non-equi-tailed 89% credible intervals, i.e. Highest Density Intervals (89% HDI), are used to describe centrality and quantify uncertainties of the regression coefficients for the individual model paths accounting for their assumed skewness. In order to disentangle the influence of the mediator depending on variations of the moderator, a conditional process analysis was employed. Specifically, conditional estimates were simulated based on posterior draws for lowest versus highest sample quintiles of mediator and moderator. To allow for inferences about the relevance of the effects, probability of direction is reported (pd) for posterior probabilities, which can be interpreted as the probability (expressed in percentage) that a parameter (described by its posterior distribution) is strictly positive or negative. The pd can take values between 50 (one half on each side) and 100 (fully on either side) and is approximated to a frequentist 2-sided p-value with the formula p-value = 2*(1-pd/100) [109, 110]. Hence, a pd of 95, 97.5, 99.5, and 99.95% corresponds to p-value at the thresholds 0.1, 0.05, 0.01, 0.001.

Acknowledgments

We thank René Clerckx for software and technical support and Paul Meugens for technical support and skillful building the technical equipment, and all volunteers for their motivation to participate.

Funding disclosure

This work was supported by the Internal Research Fund KU Leuven (PDM/15/182) and the Research Foundation Flanders (1509816N, G089818N, G0F7616N, I005018N), the Excellence of Science grant (EOS, 30446199, MEMODYN) and the KU Leuven Research Fund (C16/15/070).

Competing Interests

The authors declare that no competing interests exist.

References

1. Rozycka A, Liguz-Lecznar M. The space where aging acts: focus on the GABAergic synapse. Aging Cell. 2017; 16: 634-643. doi: 10.1111/acel.12605.
2. Buzsáki G, Geisler C, Henze DA, Wang XJ. Interneuron Diversity series: Circuit complexity and axon wiring economy of cortical interneurons. Trends Neurosci. 2004; 27: 186-193. doi: 10.1016/j.tins.2004.02.007.
3. McBain CJ, Fisahn A. Interneurons unbound. Nat Rev Neurosci. 2001; 2: 11-23. doi: 10.1038/35049047.
4. Cardin JA. Inhibitory interneurons regulate temporal precision and correlations in cortical circuits. Trends in neurosciences. 2018; 41: 689-700. doi: 10.1016/j.tins.2018.07.015.
5. Fries P. A mechanism for cognitive dynamics: neuronal communication through neuronal coherence. Trends in cognitive sciences. 2005; 9: 474-480. doi: 10.1016/j.tics.2005.08.011.
6. Fries P. Rhythms for cognition: communication through coherence. Neuron. 2015; 88: 220-235. doi: 10.1016/j.neuron.2015.09.034.
7. Heise KF, Zimerman M, Hoppe J, Gerloff C, Wegscheider K, Hummel FC. The aging motor system as a model for plastic changes of GABA-mediated intracortical inhibition and their behavioral relevance. J Neurosci. 2013; 33: 9039-9049. doi: 10.1523/JNEUROSCI.4094-12.2013.
8. Hermans L, Maes C, Pauwels L et al. Age-related alterations in the modulation of intracortical inhibition during stopping of actions. Aging (Albany NY). 2019; 11: 371-385. doi: 10.18632/aging.101741.
9. Spooner RK, Wiesman AI, Proskovec AL, Heinrichs-Graham E, Wilson TW. Rhythmic Spontaneous Activity Mediates the Age-Related Decline in Somatosensory Function. Cereb Cortex. 2019; 29: 680-688. doi: 10.1093/cercor/bhx349.
10. Marenco S, Meyer C, van der Veen JW et al. Role of gamma-amino-butyric acid in the dorsal anterior cingulate in age-associated changes in cognition. Neuropsychopharmacology. 2018; 43: 2285-2291. doi: 10.1038/s41386-018-0134-5.
11. Cassady K, Gagnon H, Lalwani P et al. Sensorimotor network segregation declines with age and is linked to GABA and to sensorimotor performance. Neuroimage. 2019; 186: 234-244. doi: 10.1016/j.neuroimage.2018.11.008.
12. Houweling S, Beek PJ, Daffertshofer A. Spectral changes of interhemispheric crosstalk during movement instabilities. Cereb Cortex. 2010; 20: 2605-2613. doi: 10.1093/cercor/bhq008.
13. Coxon JP, Goble DJ, Van Impe A, De Vos J, Wenderoth N, Swinnen SP. Reduced basal ganglia function when elderly switch between coordinated movement patterns. Cereb Cortex. 2010; 20: 2368-2379. doi: 10.1093/cercor/bhp306.
14. Baker SN, Kilner JM, Pinches EM, Lemon RN. The role of synchrony and oscillations in the motor output. Exp Brain Res. 1999; 128: 109-117. doi: 10.1007/s002210050825.
15. Brown P. Cortical drives to human muscle: the Piper and related rhythms. Prog Neurobiol. 2000; 60: 97-108. doi: 10.1016/s0301-0082(99)00029-5.
16. Mikkelsen M, Barker PB, Bhattacharyya PK et al. Big GABA: Edited MR spectroscopy at 24 research sites. Neuroimage. 2017; 159: 32-45. doi: 10.1016/j.neuroimage.2017.07.021.
17. Hermans L, Levin O, Maes C et al. GABA levels and measures of intracortical and interhemispheric excitability in healthy young and older adults: an MRS-TMS study. Neurobiology of Aging. 2018; 65: 168-177. doi: 10.1016/j.neurobiolaging.2018.01.023.
18. Maes C, Hermans L, Pauwels L et al. Age-related differences in GABA levels are driven by bulk tissue changes. Hum Brain Mapp. 2018; 39: 3652-3662. doi: 10.1002/hbm.24201.
19. Meyer-Lindenberg A, Ziemann U, Hajak G, Cohen L, Berman KF. Transitions between dynamical states of differing stability in the human brain. Proc Natl Acad Sci U S A. 2002; 99: 10948-10953. doi: 10.1073/pnas.162114799.

20. Aramaki Y, Haruno M, Osu R, Sadato N. Movement initiation-locked activity of the anterior putamen predicts future movement instability in periodic bimanual movement. J Neurosci. 2011; 31: 9819-9823. doi: 10.1523/JNEUROSCI.4473-10.2011.
21. Banerjee A, Tognoli E, Kelso JA, Jirsa VK. Spatiotemporal re-organization of large-scale neural assemblies underlies bimanual coordination. Neuroimage. 2012; 62: 1582-1592. doi: 10.1016/j.neuroimage.2012.05.046.
22. Heise KF, Monteiro TS, Leunissen I, Mantini D, Swinnen SP. Distinct online and offline effects of alpha and beta transcranial alternating current stimulation (tACS) on continuous bimanual performance and task-set switching. Sci Rep. 2019; 9: 3144. doi: 10.1038/s41598-019-39900-0.
23. Frith CD, Done DJ. Routes to action in reaction time tasks. Psychological research. 1986; 48: 169-177. doi: 10.1007/BF00309165.
24. Lakhani B, Vette AH, Mansfield A, Miyasike-daSilva V, McIlroy WE. Electrophysiological correlates of changes in reaction time based on stimulus intensity. PLoS One. 2012; 7: e36407. doi: 10.1371/journal.pone.0036407.
25. Wilkinson RT, Allison S. Age and simple reaction time: decade differences for 5,325 subjects. J Gerontol. 1989; 44: P29-35. doi: 10.1093/geronj/44.2.p29.
26. Monsell S. Task switching. Trends Cogn Sci. 2003; 7: 134-140. doi: 10.1016/S1364-6613(03)00028-7.
27. Logan GD, Bundesen C. Clever homunculus: is there an endogenous act of control in the explicit task-cuing procedure. J Exp Psychol Hum Percept Perform. 2003; 29: 575-599. doi: 10.1037/0096-1523.29.3.575.
28. Rushworth MF, Passingham RE, Nobre AC. Components of switching intentional set. J Cogn Neurosci. 2002; 14: 1139-1150. doi: 10.1162/089892902760807159.
29. Gao F, Edden RAE, Li M et al. Edited magnetic resonance spectroscopy detects an age-related decline in brain GABA levels. NeuroImage. 2013; 78: 75-82. doi: 10.1016/j.neuroimage.2013.04.012.
30. Hermans L, Leunissen I, Pauwels L et al. Brain GABA Levels Are Associated with Inhibitory Control Deficits in Older Adults. J Neurosci. 2018; 38: 7844-7851. doi: 10.1523/JNEUROSCI.0760-18.2018.
31. Cuypers K, Verstraelen S, Maes C et al. Task-related measures of short-interval intracortical inhibition and GABA levels in healthy young and older adults: A multimodal TMS-MRS study. Neuroimage. 2019; 208: 116470. doi: 10.1016/j.neuroimage.2019.116470.
32. Simmonite M, Carp J, Foerster BR et al. Age-Related Declines in Occipital GABA are Associated with Reduced Fluid Processing Ability. Acad Radiol. 2019; 26: 1053-1061. doi: 10.1016/j.acra.2018.07.024.
33. Lalwani P, Gagnon H, Cassady K et al. Neural distinctiveness declines with age in auditory cortex and is associated with auditory GABA levels. Neuroimage. 2019; 201: 116033. doi: 10.1016/j.neuroimage.2019.116033.
34. Porges EC, Woods AJ, Lamb DG et al. Impact of tissue correction strategy on GABA-edited MRS findings. Neuroimage. 2017; 162: 249-256. doi: 10.1016/j.neuroimage.2017.08.073.
35. Loehrer PA, Nettersheim FS, Jung F et al. Ageing changes effective connectivity of motor networks during bimanual finger coordination. Neuroimage. 2016; 143: 325-342. doi: 10.1016/j.neuroimage.2016.09.014.
36. Bönstrup M, Schulz R, Feldheim J, Hummel FC, Gerloff C. Dynamic causal modelling of EEG and fMRI to characterize network architectures in a simple motor task. NeuroImage. 2016; 124: 498-508. doi: 10.1016/j.neuroimage.2015.08.052.
37. Daffertshofer A, Peper CLE, Beek PJ. Stabilization of bimanual coordination due to active interhemispheric inhibition: a dynamical account. Biological Cybernetics. 2005; 92: 101-109. doi: 10.1007/s00422-004-0539-6.
38. Salenius S, Hari R. Synchronous cortical oscillatory activity during motor action. Current Opinion in Neurobiology. 2003; 13: 678-684. doi: 10.1016/j.conb.2003.10.008.
39. Feige B, Aertsen A, Kristeva-Feige R. Dynamic synchronization between multiple cortical motor areas and muscle activity in phasic voluntary movements. J Neurophysiol. 2000; 84: 2622-2629. doi: 10.1152/jn.2000.84.5.2622.

40. Muthukumaraswamy SD. High-frequency brain activity and muscle artifacts in MEG/EEG: a review and recommendations. Front Hum Neurosci. 2013; 7: 138. doi: 10.3389/fnhum.2013.00138.
41. Omlor W, Patino L, Hepp-Reymond MC, Kristeva R. Gamma-range corticomuscular coherence during dynamic force output. Neuroimage. 2007; 34: 1191-1198. doi: 10.1016/j.neuroimage.2006.10.018.
42. Johnson AN, Shinohara M. Corticomuscular coherence with and without additional task in the elderly. J Appl Physiol (1985). 2012; 112: 970-981. doi: 10.1152/japplphysiol.01079.2011.
43. Hori S, Matsumoto J, Hori E et al. Alpha- and Theta-Range Cortical Synchronization and Corticomuscular Coherence During Joystick Manipulation in a Virtual Navigation Task. Brain Topography. 2013; 26: 591-605. doi: 10.1007/s10548-013-0304-z.
44. Kapogiannis D, Reiter DA, Willette AA, Mattson MP. Posteromedial cortex glutamate and GABA predict intrinsic functional connectivity of the default mode network. NeuroImage. 2013; 64: 112-119. doi: 10.1016/j.neuroimage.2012.09.029.
45. Chen X, Fan X, Hu Y et al. Regional GABA Concentrations Modulate Inter-network Resting-state Functional Connectivity. Cereb Cortex. 2019; 29: 1607-1618. doi: 10.1093/cercor/bhy059.
46. Matsuya R, Ushiyama J, Ushiba J. Inhibitory interneuron circuits at cortical and spinal levels are associated with individual differences in corticomuscular coherence during isometric voluntary contraction. Sci Rep. 2017; 7: 44417. doi: 10.1038/srep44417.
47. Stagg CJ, Bestmann S, Constantinescu AO et al. Relationship between physiological measures of excitability and levels of glutamate and GABA in the human motor cortex. J Physiol. 2011; 589: 5845-5855. doi: 10.1113/jphysiol.2011.216978.
48. Dyke K, Pépés SE, Chen C et al. Comparing GABA-dependent physiological measures of inhibition with proton magnetic resonance spectroscopy measurement of GABA using ultra-high-field MRI. Neuroimage. 2017; 152: 360-370. doi: 10.1016/j.neuroimage.2017.03.011.
49. Hoshino O, Kameno R, Watanabe K. Reducing variability in motor cortex activity at a resting state by extracellular GABA for reliable perceptual decision-making. J Comput Neurosci. 2019; 47: 191-204. doi: 10.1007/s10827-019-00732-6.
50. Edden RAE, Muthukumaraswamy SD, Freeman TCA, Singh KD. Orientation Discrimination Performance Is Predicted by GABA Concentration and Gamma Oscillation Frequency in Human Primary Visual Cortex. Journal of Neuroscience. 2009; 29: 15721-15726. doi: 10.1523/jneurosci.4426-09.2009.
51. Puts NA, Edden RA, Evans CJ, McGlone F, McGonigle DJ. Regionally specific human GABA concentration correlates with tactile discrimination thresholds. J Neurosci. 2011; 31: 16556-16560. doi: 10.1523/JNEUROSCI.4489-11.2011.
52. Boy F, Evans CJ, Edden RA, Singh KD, Husain M, Sumner P. Individual differences in subconscious motor control predicted by GABA concentration in SMA. Curr Biol. 2010; 20: 1779-1785. doi: 10.1016/j.cub.2010.09.003.
53. Farrant M, Nusser Z. Variations on an inhibitory theme: phasic and tonic activation of GABA(A) receptors. Nat Rev Neurosci. 2005; 6: 215-229. doi: 10.1038/nrn1625.
54. Restuccia D, Valeriani M, Grassi E et al. Contribution of GABAergic cortical circuitry in shaping somatosensory evoked scalp responses: specific changes after single-dose administration of tiagabine. Clin Neurophysiol. 2002; 113: 656-671. doi: 10.1016/S1388-2457(02)00034-2.
55. Muthukumaraswamy SD, Myers JF, Wilson SJ et al. Elevating endogenous GABA levels with GAT-1 blockade modulates evoked but not induced responses in human visual cortex. Neuropsychopharmacology. 2013; 38: 1105-1112. doi: 10.1038/npp.2013.9.
56. Buffalo EA, Fries P, Landman R, Buschman TJ, Desimone R. Laminar differences in gamma and alpha coherence in the ventral stream. Proc Natl Acad Sci U S A. 2011; 108: 11262-11267. doi: 10.1073/pnas.1011284108.
57. Traub RD, Hawkins K, Adams NE, Hall SP, Simon A, Whittington MA. Layer 4 pyramidal neuron dendritic bursting underlies a post-stimulus visual cortical alpha rhythm. Commun Biol. 2020; 3: 230. doi: 10.1038/s42003-020-0947-8.

58. Adams NE, Hughes LE, Phillips HN et al. GABA-ergic Dynamics in Human Frontotemporal Networks Confirmed by Pharmaco-Magnetoencephalography. J Neurosci. 2020; 40: 1640-1649. doi: 10.1523/JNEUROSCI.1689-19.2019.
59. Wu X, Huang L, Wu Z et al. Homeostatic competition between phasic and tonic inhibition. J Biol Chem. 2013; 288: 25053-25065. doi: 10.1074/jbc.M113.491464.
60. Leventhal AG. GABA and Its Agonists Improved Visual Cortical Function in Senescent Monkeys. Science. 2003; 300: 812-815. doi: 10.1126/science.1082874.
61. Schmolesky MT, Wang Y, Pu M, Leventhal AG. Degradation of stimulus selectivity of visual cortical cells in senescent rhesus monkeys. Nat Neurosci. 2000; 3: 384-390. doi: 10.1038/73957.
62. Hall SD, Stanford IM, Yamawaki N et al. The role of GABAergic modulation in motor function related neuronal network activity. Neuroimage. 2011; 56: 1506-1510. doi: 10.1016/j.neuroimage.2011.02.025.
63. Ratcliff R, Thapar A, McKoon G. Application of the diffusion model to two-choice tasks for adults 75-90 years old. Psychology and aging. 2007; 22: 56. doi: 10.1037/0882-7974.22.1.56.
64. Hoshino O, Zheng M, Watanabe K. Reduction of trial-to-trial perceptual variability by intracortical tonic inhibition. Neural computation. 2016; 28: 187-215. doi: 10.1162/NECO_a_00799.
65. King BR, van Ruitenbeek P, Leunissen I et al. Age-Related Declines in Motor Performance are Associated With Decreased Segregation of Large-Scale Resting State Brain Networks. Cereb Cortex. 2018; 28: 4390-4402. doi: 10.1093/cercor/bhx297.
66. Moezzi B, Pratti LM, Hordacre B et al. Characterization of Young and Old Adult Brains: An EEG Functional Connectivity Analysis. Neuroscience. 2019; 422: 230-239. doi: 10.1016/j.neuroscience.2019.08.038.
67. Wang B, Li P, Li D et al. Increased Functional Brain Network Efficiency During Audiovisual Temporal Asynchrony Integration Task in Aging. Front Aging Neurosci. 2018; 10: 316. doi: 10.3389/fnagi.2018.00316.
68. Michely J, Volz LJ, Hoffstaedter F et al. Network connectivity of motor control in the ageing brain. Neuroimage Clin. 2018; 18: 443-455. doi: 10.1016/j.nicl.2018.02.001.
69. Oldfield RC. The assessment and analysis of handedness: The Edinburgh inventory. Neuropsychologia. 1971; 9: 97-113. doi: 10.1016/0028-3932(71)90067-4.
70. Yousry TA, Schmid UD, Alkadhi H et al. Localization of the motor hand area to a knob on the precentral gyrus. A new landmark. Brain. 1997; 120: 141-157. doi: 10.1093/brain/120.1.141.
71. Baumgarten TJ, Oeltzschner G, Hoogenboom N, Wittsack HJ, Schnitzler A, Lange J. Beta Peak Frequencies at Rest Correlate with Endogenous GABA+/Cr Concentrations in Sensorimotor Cortex Areas. PLoS One. 2016; 11: e0156829. doi: 10.1371/journal.pone.0156829.
72. Mescher M, Merkle H, Kirsch J, Garwood M, Gruetter R. Simultaneous in vivo spectral editing and water suppression. NMR in Biomedicine: An International Journal Devoted to the Development and Application of Magnetic Resonance In Vivo. 1998; 11: 266-272.
73. Edden RA, Puts NA, Harris AD, Barker PB, Evans CJ. Gannet: A batch-processing tool for the quantitative analysis of gamma-aminobutyric acid–edited MR spectroscopy spectra. J Magn Reson Imaging. 2014; 40: 1445-1452. doi: 10.1002/jmri.24478.
74. Near J, Edden R, Evans CJ, Paquin R, Harris A, Jezzard P. Frequency and phase drift correction of magnetic resonance spectroscopy data by spectral registration in the time domain. Magn Reson Med. 2015; 73: 44-50. doi: 10.1002/mrm.25094.
75. Mikkelsen M, Rimbault DL, Barker PB et al. Big GABA II: Water-referenced edited MR spectroscopy at 25 research sites. Neuroimage. 2019; 191: 537-548. doi: 10.1016/j.neuroimage.2019.02.059.
76. Rothman DL, Petroff OA, Behar KL, Mattson RH. Localized 1H NMR measurements of gamma-aminobutyric acid in human brain in vivo. Proc Natl Acad Sci U S A. 1993; 90: 5662-5666. doi: 10.1073/pnas.90.12.5662.
77. Edden RAE, Puts NAJ, Barker PB. Macromolecule-suppressed GABA-edited magnetic resonance spectroscopy at 3T. Magnetic resonance in medicine. 2012; 68: 657-661. doi: 10.1002/mrm.24391.

78. Harris AD, Puts NAJ, Edden RAE. Tissue correction for GABA-edited MRS: Considerations of voxel composition, tissue segmentation, and tissue relaxations. Journal of Magnetic Resonance Imaging. 2015; 42: 1431-1440. doi: 10.1002/jmri.24903.
79. Schöner G, Kelso JA. Dynamic pattern generation in behavioral and neural systems. Science. 1988; 239: 1513-1520. doi: 10.1126/science.3281253.
80. Delorme A, Makeig S. EEGLAB: an open source toolbox for analysis of single-trial EEG dynamics including independent component analysis. J Neurosci Methods. 2004; 134: 9-21. doi: 10.1016/j.jneumeth.2003.10.009.
81. Oostenveld R, Fries P, Maris E, Schoffelen JM. FieldTrip: Open source software for advanced analysis of MEG, EEG, and invasive electrophysiological data. Comput Intell Neurosci. 2011; 2011: 156869. doi: 10.1155/2011/156869.
82. Gomez-Herrero G, De Clercq W, Anwar H et al. Automatic Removal of Ocular Artifacts in the EEG without an EOG Reference Channel. Proceedings of the 7th Nordic Signal Processing Symposium - NORSIG 2006. 2006; doi: 10.1109/norsig.2006.275210.
83. Chaumon M, Bishop DVM, Busch NA. A practical guide to the selection of independent components of the electroencephalogram for artifact correction. Journal of Neuroscience Methods. 2015; 250: 47-63. doi: 10.1016/j.jneumeth.2015.02.025.
84. McClelland VM, Cvetkovic Z, Mills KR. Rectification of the EMG is an unnecessary and inappropriate step in the calculation of Corticomuscular coherence. Journal of Neuroscience Methods. 2012; 205: 190-201. doi: 10.1016/j.jneumeth.2011.11.001.
85. Schoffelen J-M. Neuronal Coherence as a Mechanism of Effective Corticospinal Interaction. Science. 2005; 308: 111-113. doi: 10.1126/science.1107027.
86. Myers LJ, Lowery M, O'Malley M et al. Rectification and non-linear pre-processing of EMG signals for cortico-muscular analysis. J Neurosci Methods. 2003; 124: 157-165. doi: 10.1016/s0165-0270(03)00004-9.
87. Iacono MI, Neufeld E, Akinnagbe E et al. MIDA: A Multimodal Imaging-Based Detailed Anatomical Model of the Human Head and Neck. PLOS ONE. 2015; 10: e0124126. doi: 10.1371/journal.pone.0124126.
88. Samogin J, Liu Q, Marino M, Wenderoth N, Mantini D. Shared and connection-specific intrinsic interactions in the default mode network. NeuroImage. 2019; 200: 474-481. doi: 10.1016/j.neuroimage.2019.07.007.
89. Liu Q, Ganzetti M, Wenderoth N, Mantini D. Detecting Large-Scale Brain Networks Using EEG: Impact of Electrode Density, Head Modeling and Source Localization. Front Neuroinform. 2018; 12: 4. doi: 10.3389/fninf.2018.00004.
90. Liu Q, Farahibozorg S, Porcaro C, Wenderoth N, Mantini D. Detecting large-scale networks in the human brain using high-density electroencephalography. Hum Brain Mapp. 2017; 38: 4631-4643. doi: 10.1002/hbm.23688.
91. Taberna GA, Marino M, Ganzetti M, Mantini D. Spatial localization of EEG electrodes using 3D scanning. J Neural Eng. 2019; 16: 026020. doi: 10.1088/1741-2552/aafdd1.
92. Haueisen J, Ramon C, Eiselt M, Brauer H, Nowak H. Influence of tissue resistivities on neuromagnetic fields and electric potentials studied with a finite element model of the head. IEEE Transactions on Biomedical Engineering. 1997; 44: 727-735. doi: 10.1109/10.605429.
93. Vorwerk J, Aydin U, Wolters CH, Butson CR. Influence of Head Tissue Conductivity Uncertainties on EEG Dipole Reconstruction. frontiers in Neuroscience. 2019; 13: 531. doi: 10.3389/fnins.2019.00531.
94. Wolters CH, Grasedyck L, Hackbusch W. Efficient computation of lead field bases and influence matrix for the FEM-based EEG and MEG inverse problem. Inverse Problems. 2004; 20: 1099-1116. doi: 10.1088/0266-5611/20/4/007.
95. Pascual-Marqui RD. Discrete, 3D distributed, linear imaging methods of electric neuronal activity. Part 1: exact, zero error localization. arXiv preprint arXiv:07103341. 2007;
96. Lachaux J-P, Rodriguez E, Le Van Quyen M, Lutz A, Martinerie J, Varela FJ. Studying single-trials of phase synchronous activity in the brain. International Journal of Bifurcation and Chaos. 2000; 10: 2429-2439. doi: 10.1142/S0218127400001560.

97. Tallon-Baudry, Bertrand. Oscillatory gamma activity in humans and its role in object representation. Trends Cogn Sci. 1999; 3: 151-162. doi: 10.1016/s1364-6613(99)01299-1.
98. Cohen MX. A better way to define and describe Morlet wavelets for time-frequency analysis. Neuroimage. 2019; 199: 81-86. doi: 10.1016/j.neuroimage.2019.05.048.
99. Mormann F, Lehnertz K, David P, E. Elger C. Mean phase coherence as a measure for phase synchronization and its application to the EEG of epilepsy patients. Physica D: Nonlinear Phenomena. 2000; 144: 358-369. doi: 10.1016/s0167-2789(00)00087-7.
100. Ciuparu A, Mureşan RC. Sources of bias in single-trial normalization procedures. Eur J Neurosci. 2016; 43: 861-869. doi: 10.1111/ejn.13179.
101. Funder DC, Ozer DJ. Evaluating effect size in psychological research: Sense and nonsense. Advances in Methods and Practices in Psychological Science. 2019; 2: 156-168. doi: 10.1177/2515245919847202.
102. Chen H, Cohen P, Chen S. How big is a big odds ratio? Interpreting the magnitudes of odds ratios in epidemiological studies. Communications in Statistics—simulation and Computation®. 2010; 39: 860-864. doi: 10.1080/03610911003650383.
103. Maris E, Oostenveld R. Nonparametric statistical testing of EEG- and MEG-data. Journal of Neuroscience Methods. 2007; 164: 177-190. doi: 10.1016/j.jneumeth.2007.03.024.
104. Yuan Y, MacKinnon DP. Bayesian mediation analysis. Psychol Methods. 2009; 14: 301-322. doi: 10.1037/a0016972.
105. Carpenter B, Gelman A, Hoffman MD et al. Stan: A Probabilistic Programming Language. Journal of Statistical Software. 2017; 76: 10.18637/jss.v076.i01.
106. Bürkner P-C. brms: An R Package for Bayesian Multilevel Models Using Stan. Journal of Statistical Software. 2017; 80: 1-28. doi: 10.18637/jss.v080.i01.
107. Bürkner P-C. Advanced Bayesian Multilevel Modeling with the R Package brms. The R Journal. 2018; 10: 395. doi: 10.32614/rj-2018-017.
108. Goodrich B GJ, Ali I & Brilleman S. rstanarm: Bayesian applied regression modeling via Stan. R package version 2.19.3. 2020;
109. Makowski D, Ben-Shachar M, Lüdecke D. bayestestR: Describing Effects and their Uncertainty, Existence and Significance within the Bayesian Framework. Journal of Open Source Software. 2019; 4: 1541. doi: 10.21105/joss.01541.
110. Makowski D, Ben-Shachar MS, Chen SHA, Lüdecke D. Indices of Effect Existence and Significance in the Bayesian Framework. Front Psychol. 2019; 10: 2767. doi: 10.3389/fpsyg.2019.02767.

Supporting Information

Figure S1	Consistency of the MRS voxel placement across participants and individual traces of edited spectra for each voxel.
Table S1	Overview of the descriptive statistics of GABA+ and quantitative quality.
Table S2	Analysis of deviance table for backwards selection of parameters predicting GABA+.
Table S3	Results for Gamma GLMM predicting GABA+. Summary of model estimated marginal means contrasts for effect of group by voxel interaction on GABA+ levels.
Figure S3	Effect of quality metrics on GABA as included in the final model.
Table S4	Results for logistic GLMM to predict failed transitions [trials with 100% error rate].
Table S5	Results for logistic GLMM to predict fully correct transitions [trials with 0% error]. Summary of model estimated marginal means contrasts for the effect of age group × coordination pattern× transition condition interaction on fully correct transitions [trials with 0% error].
Table S6	Results for beta GLMM to predict cumulative error rate [0<error rate/100 <1]. Summary of model estimated marginal means contrasts for the effect of the transition condition by age group interaction on cumulative error rate.
Table S7	Results for gamma GLMM to predict transition latency. Summary of model estimated marginal means contrasts for the effect of the age group by transition condition interaction on transition latency.
Table S8	Thumb reaction time (tRT) – Operationalization and Statistical analysis. Results for gamma GLMM to predict thumb reaction time.
Figure S9	Stimulus-locked analysis of power change relative to baseline. Statistical results of cluster corrected permutation test for significant power changes from baseline.
Figure S10	Statistical results of cluster corrected permutation test for power changes.
Figure S11	Stimulus-locked analysis of ISPC modulation.
Table S12	Results of Bayesian moderated mediation analysis for the association between behavior, cortico-cortical connectivity, and GABA+.
Table S13	Results of Bayesian moderated mediation analysis for the association between behavior, cortico-spinal connectivity, and GABA+ on the dominant side (left M1-right FDI zISPC).
Table S14	Results of Bayesian moderated mediation analysis for the association between behavior, cortico-spinal connectivity, and GABA+ on the non-dominant side (right M1- left FDI zISPC).